Nonlinear Optical Fibres for UV and Infrared Generation

Harris, Jonathan

Award date:
2020

Awarding institution:
University of Bath

Nonlinear Optical Fibres for UV and Infrared Generation

Jonathan E. Harris
University of Bath

Submitted for the degree of Doctor of Philosophy
August 2019

Supervised by
Prof. William J. Wadsworth

Centre for Photonics and Photonic Materials
Department of Physics
University of Bath
United Kingdom

for Maria.

Abstract

The research presented in this thesis is in three parts. First is an investigation into the generation of supercontinuum using tapered optical fibre. Second, is the creation of side-holes in hollow-core fibre, using an oxygen-butane flame, with the aim to be used for gas sensing. Finally, variables affecting the amount of power in a near infrared idler, of a four-wave mixing fibre were explored.

Supercontinuum generation is most commonly generated using photonic crystal fibre. The purpose of this research is not to provide alternative to photonic crystal fibre but to investigate some of the processes that affect supercontinuum generation that utilises soliton fission. Using a master oscillator power amplifier to deliver a 1064 nm pump, it was found that supercontinuum could be generated using tapered optical fibre with a waist length under 250 mm, even though the pulses were as long as 10 ps. The tapers were made using the flame brush technique which allows the creation of tapers with micrometer diameters. These tapers are connected at either end by standard/full size optical fibres. This presents an opportunity to investigate taper waists of many designs whilst keeping the input and output wavelength dependence of coupling independent of the taper structure, unlike in photonic crystal fibres. Investigating the limits of soliton trapping led to non-uniform designs of taper waists. The design with the broadest spectrum began with a 5 μm diameter that was connected directly to a 2.5 μm section. This allowed dispersive waves to be generated, with decent power, in the 5 μm section before the change in group velocity induced by the 2.5 μm diameter, coupled with soliton trapping, dragged the dispersive to low wavelengths. This design produced a supercontinuum, that maintained a power level above -30 dBm, over a range of 420 - 1550 nm.

Using hollow-core fibres for gas sensing is an active area of interest. Side-holes allow gases to enter the core of the fibre in order to be detected. Ultrafast lasers are the most common tool when creating these holes. Here an alternate method of using an oxygen-butane flame on a pressurised hollow-core fibre was investigated. It was found that reducing the inner diameter of the burner, delivering gases to the flame, can only reduce the size of the flame to ≈300 μm. Side-holes were successfully created on a hollow-core fibre of 125 μm diameter. However the minimum loss from a hole created this way was 3 dB which makes this method unsuitable for detection of gases over large areas.

A master oscillator power amplifier laser system was used to deliver a 1064 nm pump to a photonic crystal fibre with an phase matched idler of 1915 nm. The width of the pulses was varied between 37 - 90 ps and had their maximum peak powers kept around 2200 W. The long width of these pulses allowed a narrow bandwidth that produced an idler peak that had a full width at half maximum of ≈30 nm. Three pulse repetition rates of 40, 20 and 10 MHz were used and the maximum average power adjusted in order to keep the same peak power. Over 100 mW of idler power was generated. It was found that the relation of peak power to length of fibre needed to generate power in the idler, is complicated by confinement loss of the idler. This means that to generate the most power the fibre should be short and the peak power of the pulse large.

Contents

Chapter 1

Introduction

This thesis contains an investigation into the generation of supercontinuum using optical fibres that have been tapered down into silica microwires. It has been over 50 years since the first report of supercontinuum generation (Stoicheff 1963) and it is still an area of high interest. I believe the continued attraction can be attributed to two simple but important points;

- The progression of technology is continuing to improve the level of control over supercontinuum generation whilst simultaneously reducing cost of equipment. Development in laser systems is particularly significant allowing finer control of pulse parameters. Optical fibres fabrication has also progressed leading to novel designs that allow better manipulation of propagation properties such as dispersion.

- Supercontinuum light sources have a large range of applications. These

include frequency comb metrology (Carlson et al. 2017, Ye et al. 2003), gas and chemical sensing (Kaminski et al. 2008, Ere-Tassou et al. 2003), communications (Takara et al. 2005) and more.

For soliton-fission driven supercontinuum generation, two common methods are the use of photonic crystal fibres (Knight et al. 1997, Stone et al. 2016) and standard fibres that have been tapered down into microwires (Birks et al. 2000). Both of these methods use high-index step and small cores to allow manipulation of the fibre dispersion. Photonic crystal fibres have been used in the generation of supercontinuum since Ranka et al. (2000) used them to fabricate a fibre with a zero dispersion wavelength around 770 nm. Later that year it was shown by Birks et al. (2000) that the dispersion engineering allowed by photonic crystal fibres could be replicated by tapering standard telecommunications fibre. Tapering down to a diameter of 2 μm, continuum of similar bandwidth as that seen in photonic crystal fibres was observed. Tapering standard optical fibres to change nonlinear properties was actually suggested by Dumais et al. (1993) both experimentally and numerically however, the potential for supercontinuum generation was not noted as the pump wavelength was too long.

Although not explored in this thesis the use of non-oxide glasses for supercontinuum generation is a very promising as some of these glasses are transparent over much larger bandwidths than silica glass, especially in the

infra-red region. Wang et al. (2018) tapered a fibre formed of an As_2Se_3 core and As_2S_3 cladding to generate supercontinuum spanning 1.9 - 5.7 μm and Swiderski et al. (2018) used ZBLAN glass to fabricate fibre that generated supercontinua with a spectral flatness of 2 dB over 1710 nm of bandwidth.

The method of supercontinuum generation used in this thesis involves the tapering of a section of standard optical fibre such that to either side of the tapered section there is unaffected fibre. This leads to the uniqueness of the supercontinuum work in this thesis; There is a large quantity of directly comparable data. When comparing supercontinua from different photonic crystal fibres it is important to remember that the input and output coupling will be different thus making direct comparison complicated. This is due to the core size of the photonic crystal fibres influencing the numerical aperture. By keeping fibre on either side of the tapered section the same between experiments then differences in results can be attributed to the tapered section. Having comparable data like this allows a thorough investigation of supercontinuum generating tapers.

An investigation into creating side-holes in hollow-core optical fibre using an oxygen-butane flame is also within this thesis with hope for future application in gas sensing. Using hollow core optical fibre for gas sensing is an area of interest in scientific research (Yang et al. 2014, Wojcik et al. 1999, Masum et al. 2018, Sardar & Faisal 2017). To allow gases to enter the core, holes

can be created in the side of the fibre. These holes have been created using laser drilling and is now a proven technique (Karp et al. 2016, Lehmann et al. 2010, Urich et al. 2012). The investigation in this report will look at using a premixed oxygen-butane flame instead of lasers to drill the holes. This alternative could provide a method that is simpler and cheaper to mass produce than using laser drilling. This investigation began by creating as small a flame as possible using premixed oxygen-butane. Flames of very small size have use as ionization detectors in gas chromatography (McWilliam & Dewar 1958), such as those used by Thurbide & Hayward (2004) to create a flame of ≈3 mm diameter using a 0.254 mm inner-diameter stainless steel capillary burner. Flame spectrometry is another use for small flames (Zimmermann et al. 2000). The author of this thesis is unaware of any previous work in using premixed oxygen-butane flames to create side-holes in hollow-core optical fibre.

This thesis also contains an investigation into four-wave mixing with a focus on generating significant power in a mid-infrared idler by investigating the effects of pulse repetition rate and pulse duration. The pump laser produced pulses that were tens of picoseconds long, had narrow bandwidth and were not transform limited. Previous work at the University of Bath showed that it was possible to achieve 30% conversion efficiency to the signal wavelength using a similar photonic crystal fibre with picosecond pulses (Lavoute et al. 2010, Yarrow et al. 2012, Nodop et al. 2009).

Four-wave mixing is commonly used for many applications such as in telecommunications as a method of converting wavelengths without losing information (Lu et al. 2006, Chen & Gao 2015, Awang et al. 2010). Another reason for four-wave mixing's popularity is the control it can allow over the properties of resultant idler and signal including the possibility of maintaining polarisation (Morioka et al. 1994, Chu et al. 2010, Zuo et al. 2010). The work in this thesis looks at generating an idler with a wavelength just below 2000 nm which is similar to the wavelength of many thulium based solid states lasers (Kracht et al. 2016, Wang et al. 2019). Using four-wave mixing to generate wavelengths in the mid-infrared is currently attractive as, in the region near 2 μm, it provides an alternate to the somewhat expensive thulium components found in some mid-infrared lasers (Zhang et al. 2016, Jin et al. 2019).

Chapter 2

Background Theory

2.1 Optical Fibres

Optical fibre is a waveguide for light usually made of glass. Guiding light has many uses including faster internet connections than those using copper wire. This is due to optical fibre having a much wider frequency range and lower loss which means that signals can travel much further before they must be repeated. The most common optical fibre consists of a rod of glass (the core) surrounded by another layer of glass (the cladding). The core and cladding have different refractive indices from one another ($n_{\text{cladding}} < n_{\text{core}}$) due to intentional impurities in the glass such as germanium or fluorine. Refractive index is the ratio of the speed of light in a vacuum and the speed of light in the medium (Foster et al. 2005).

For an optical fibre to guide light in the core then we have to understand

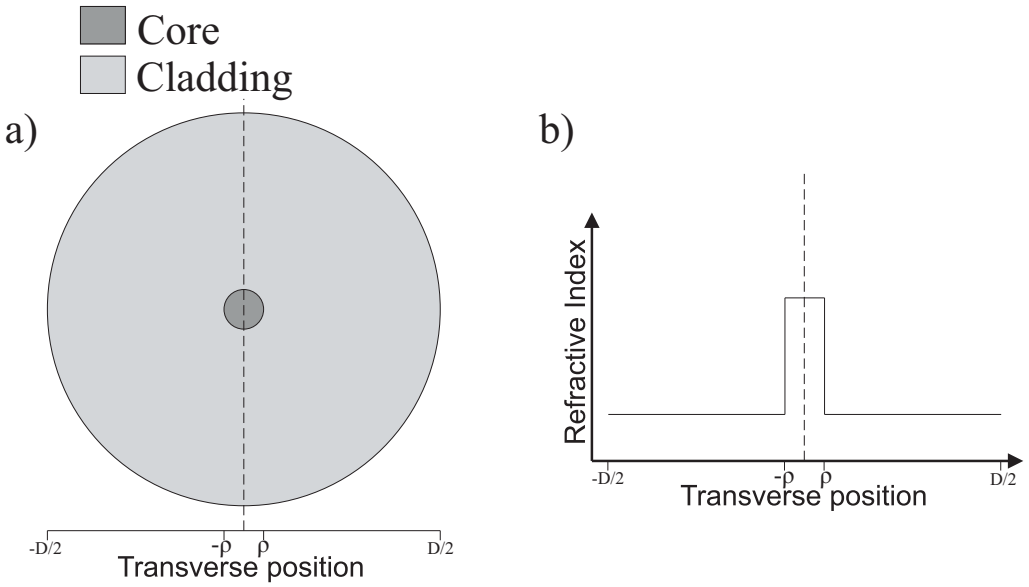

Figure 2.1 a) Diagram of the transverse section of a fibre. b) Refractive index profile for the fibre in a). ρ is the core radius and D is the cladding diameter.

what will happen when light reaches the boundary between the core and cladding. Due to the difference in refractive index, the light will either be refracted or reflected. Snell's law describes refraction and critical angle which gives the conditions for total internal reflection(Tipler & Mosca 2007, p.1042),

$$\sin\theta_{\text{crit}} = \frac{n_{\text{clad}}}{n_{\text{core}}}, \tag{2.1}$$

where θ_{crit} is the critical angle of incidence. Light in the core hitting the core/cladding interface with an angle that is greater than the critical angle of the two mediums will be reflected back into the core. This leads to the light

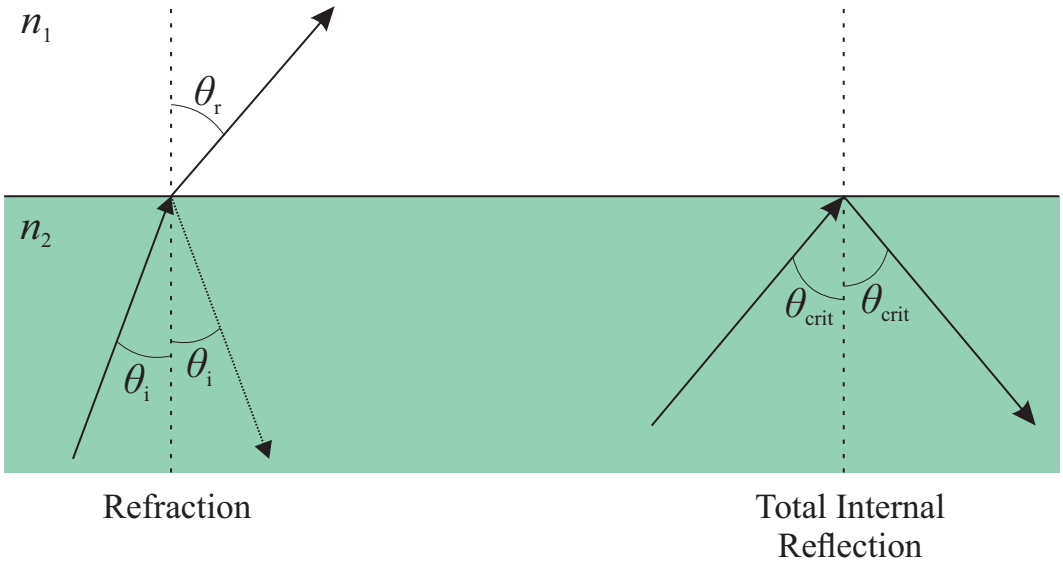

Figure 2.2 Diagram showing a ray of light reaching the boundary between 2 mediums of refractive index n_1 and n_2.

being trapped inside the core and unable to escape into the cladding. Over time, and with a great many reflections, light will travel along the length of the optical fibre.

2.2 Fibre Fabrication

The University of Bath has a fibre drawing tower which is used for the fabrication of many types of fibre including photonic crystal and hollow-core (Ortigosa-Blanch et al. 2000, Yu et al. 2012). Fibres are made from what is known as a preform which is essentially an enlarged version, typically a meter in length and 20 - 40 mm in diameter. The preform has the same transverse refractive index profile of the desired fibre but scaled up, that is the ratio

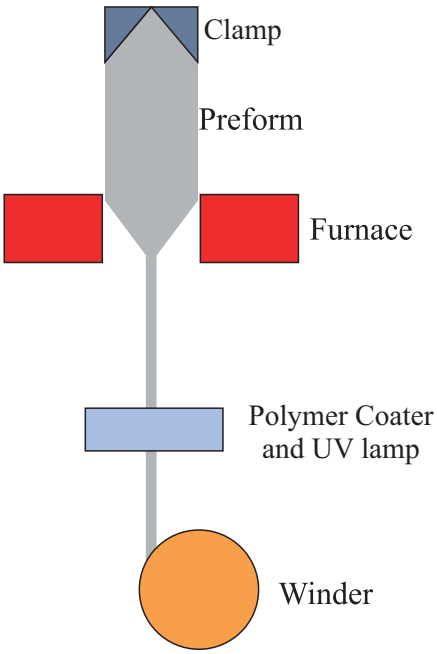

Figure 2.3 Diagram showing the basic principle of the fibre drawing tower.

between the diameter of the core and the diameter of the cladding.

The preform is held at the top of the fibre drawing tower by a clamp. The preform is lowered until the bottom enters a cylindrical furnace with a temperature around 2000 °C. The part of the preform within the furnace will soften and can be pulled out of the furnace without detaching it. If it is pulled out of the furnace at a higher rate than it is being lowered then it will stretch and become thinner whilst still maintaining the cross sectional refractive index profile. The pulling of the preform is done by a winder whose speed can be controlled by a computer. By adjusting the speed of the winder and the feed rate of the preform, a fibre of the desired diameter can be made. The fibre is

still susceptible to damage however and so between the furnace and the winder a UV curing polymer is applied to the outside. Once the polymer is applied, a UV lamp is used to allow it to harden. A diagram of this process is shown in figure (2.3).

2.3 Waveguide Modes

Total internal reflection is a useful way of visualising how light moves in a fibre but is only accurate for waveguides where the core is much larger than the wavelength of the light. To properly understand how light moves in a fibre we need to use Maxwell's equations (Silfvast 2004, p.12),

$$\nabla \times \mathbf{E} = -\frac{\partial \mathbf{B}}{\partial t}, \tag{2.2}$$

$$\nabla \times \mathbf{H} = \mathbf{J} + \frac{\partial \mathbf{D}}{\partial t}, \tag{2.3}$$

$$\nabla \cdot \mathbf{D} = \rho_f, \tag{2.4}$$

$$\nabla \cdot \mathbf{B} = 0. \tag{2.5}$$

where **E** is the electric field, **H** is the magnetic field, **D** is the displacement current density, **B** is the magnetic flux density, **J** is the current density and ρ_f is the charge density. For the case of an optical fibre made of glass there is no free charges so ρ_f and **J** are both equal to zero. A mode will have an electric field of the form

$$\mathbf{E}(x, y, z, t) = \mathbf{E}(x, y)e^{i(\beta z - \omega t)}, \tag{2.6}$$

where β is the propagation constant which is the wavevector component along the direction of propagation and ω is the angular frequency of the wave. Using vector identities it is possible to manipulate Maxwell's equations to give the wave equation. Subbing in equation (2.6)

$$\nabla_T^2\mathbf{E} + (k^2 n(x, y)^2 - \beta^2)\mathbf{E} = -(\nabla_T + i\beta z)(\mathbf{E} \cdot \nabla_T ln(n^2)), \tag{2.7}$$

where k is the angular wavenumber and $\nabla_T = (\frac{1}{x}, \frac{1}{y}, 0)$. This is difficult to solve as the right hand side shows that the x and y components of **E** are coupled together but this side can be neglected entirely if $\Delta(n) \ll n$. This is known as the weak guidance approximation. Equation (2.7) can be written as

$$\mathbf{E}(x, y) = \Psi(x, y)e^{)i(\beta z - \omega t)}\hat{\mathbf{e}}_t, \tag{2.8}$$

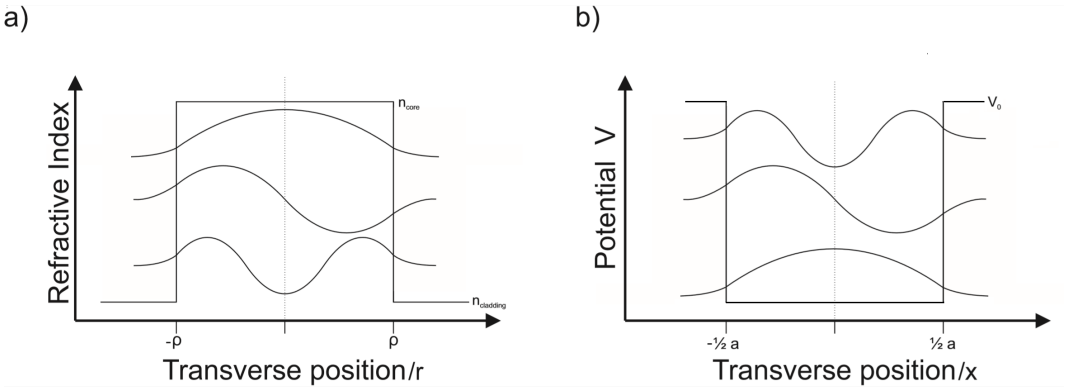

Figure 2.4 a) Mode field distributions inside a step-index fibre. b) The wave functions of a particle inside a potential well with depth V_0 and with a width of a.

where Ψ is the scalar field of $\mathbf{E}(x, y)$ and $\hat{\mathbf{e}}_t$ is a constant transverse vector. Subbing equation (2.8) into equation (2.7) and neglecting the right hand side we get the scalar wave equation

$$\nabla_T^2 \Psi + (k^2 n^2 - \beta^2)\Psi = 0. \tag{2.9}$$

The scalar wave equation is formally identical to Schrödinger's equation from quantum mechanics with the wave function of a particle being the mode field distribution of the wave, probability density equivalent to intensity and the size of the potential well to the refractive index step. The solution to equation (2.9) is shown in figure (2.4 a) with the wavefunctions of bound states shown in (2.4) (b) for comparison.

Solving the Schrödinger equation for a finite potential well shows that there exists a finite number of energy levels that a particle can occupy. It is the

same when solving for modes in a step-index fibre where the energy levels in the potential well are now comparable to the propagation constants of the allowed modes of the fibre. The solution with the largest propagation constant is known as the fundamental mode and in single-moded fibres it is only this mode that can propagate. When finding the number of modes that a fibre can support it is useful to find the V-number also known as the fibre parameter

$$V = \frac{2\pi\rho}{\lambda} NA, \tag{2.10}$$

where ρ is the core radius and NA is the numerical aperture of the fibre that is a dimensionless number that is the sine of the maximum angle that light can be incident upon the fibre and still be trapped in the core. If $V < 2.405$ then the fibre will only guide the fundamental mode and if $V \gg 1$ then the number of modes that the fibre can support is estimated with $N \approx \frac{V^2}{4}$.

2.4 Dispersion

Light that is propagating in a fibre will travel with a group velocity that is dependent on its wavelength. This phenomena is known as dispersion. When a prism breaks white light into a rainbow of wavelengths, it is dispersion that is responsible as each wavelength will experience a different refractive index as it passes through the prism.

There are two main types of dispersion, waveguide and material. To

understand waveguide dispersion it is first important to understand that propagating modes experience an effective refractive index, n_{eff}

$$n_{\text{eff}} = \frac{\beta}{k}. \tag{2.11}$$

For a mode propagating in the core of a standard step-index fibre $n_{\text{clad}} < n_{\text{eff}} < n_{\text{core}}$. It is this difference between the refractive index that gives rise to waveguide dispersion. This is mainly dependent upon the physical dimensions of the fibre and difference in refractive index between the core and the cladding.

Material dispersion is related to the refractive index of a material being frequency dependent $n(\omega)$. This means that a propagating pulse will spread out temporally due to the frequencies that it is made up of travelling at different speeds. The group velocity of a pulse is defined as

$$v_g = \frac{\mathrm{d}\omega}{\mathrm{d}\beta}. \tag{2.12}$$

The time taken for a pulse to travel a distance L is therefore

$$\tau = \frac{L}{v_g} = L\frac{\mathrm{d}\beta}{\mathrm{d}\omega} = L\beta_1, \tag{2.13}$$

where

$$\beta_1 = \frac{\mathrm{d}\beta}{\mathrm{d}\omega} = \frac{1}{v_g}. \tag{2.14}$$

So if a pulse consists of frequencies from ω to $\omega + \delta\omega$ then the difference in time taken for the frequencies to travel the distance L will be separated by

$$\delta\tau = L\beta_1(\omega + \delta\omega) - L\beta_1(\omega) = L\delta\omega\frac{\mathrm{d}\beta_1}{\mathrm{d}\omega}. \tag{2.15}$$

$\beta_2 = \frac{\mathrm{d}\beta_1}{\mathrm{d}\omega}$ and is known as the group velocity dispersion. It is common to describe dispersion in terms of wavelength with the variable D where (Meschede 2017)

$$D = \frac{\mathrm{d}(\frac{1}{v_g})}{\mathrm{d}\lambda} = -\delta\omega\frac{\mathrm{d}\beta_1}{\mathrm{d}\omega}. \tag{2.16}$$

The variable D will have an opposite sign than β_2 so in order to avoid confusion when $D < 0$ and $\beta_2 > 0$ this is called normal dispersion whereas when $D > 0$ and $\beta_2 < 0$ the pulse is in the anomalous dispersion regime. A pulse undergoing normal dispersion will find its longer wavelengths travelling faster than the shorter wavelengths whereas if it is anomalous dispersion this effect is reversed.

The point at which β_2 and D are both zero is known as the zero dispersion wavelength where no dispersion occurs. The dispersion length gives a scale over which a pulse will experience significant dispersion and is defined as

$$L_D = \frac{T_0}{|\beta_2|}, \tag{2.17}$$

where T_0 is the pulse duration.

Manipulation of a waveguide's dispersion is important in supercontinuum generation and is discussed in more detail in section (2.7.1) of this thesis.

2.5 Nonlinearity

The Kerr effect is where the refractive index changes due to the presence of an electric field. When the electric field is applied externally then it is known as the Kerr electro-optic effect and when the change in refractive index is due to the electric field of a propagating wave then it is known as the optical Kerr effect. The optical Kerr effect changes the refractive index linearly in relation to the intensity of the electromagnetic wave

$$n_{tot} = n + n_2 I, \tag{2.18}$$

where n_2 is the nonlinear refractive index. The Kerr effect is not the only contribution to the nonlinear refractive index as an effect known as electrostriction can also have a significant influence. Electrostriction will not be discussed in detail here but a short summation would be that the electric field of the propagating wave causes density variations in the material.

The Kerr effect is responsible for several nonlinear effects such as self-phase modulation and Kerr lensing. As the optical Kerr effect is related to the intensity of the electric field it is strongest at the centre of a laser beam and becomes weaker further away. Therefore the total refractive index is highest in

the centre and can act like a lens focusing a beam towards the centre. When this happens to a pulse, its effective mode area is decreased, as it is focused towards the area of highest refractive index. When this happens to a pulse it is said to be self-focussing.

The optical Kerr effect also leads to a pulse undergoing a change in its phase and as this is caused by the electric field of the pulse it is known as self-phase modulation. The rise in refractive index caused by the optical Kerr effect is directly related to the intensity of the electric field present. This means that, because of the intensity distribution, the leading edge of a pulse will experience a lower refractive index than that of the centre before its falls again over the trailing edge of the pulse. It is this variation of refractive index that causes the phase change during the pulse. The strength of the phase shift caused by self-phase modulation is therefore proportional to the rate of change of intensity with time. The change in index, responsible for self-phase modulation, can also be caused by the electric field of another propagating pulse. When this happens it is known as cross-phase modulation.

The effect on a pulse undergoing self-phase modulation is that the leading edge will be red-shifted into longer wavelengths whereas the trailing edge will be blue-shifted. Without taking into consideration any dispersive effects this would just lead to spectral broadening. However, in the presence of normal dispersion, self-phase modulation causes a pulse to become longer as the

leading red-shifted edge of the pulse can travel faster than the trailing blue-shifted edge. If the dispersion is in the anomalous regime then the effects of self-phase modulation can cancel out the spreading caused by the dispersion to form solitons, which will be discussed in section (2.7).

Stimulated Raman scattering and stimulated Brillouin scattering are two nonlinear processes that impart part off the energy of the electromagnetic wave to the medium through inelastic collisions. Although both involve inelastic scattering, the difference between the two lies in that stimulated Raman scattering involves optical phonons whereas stimulated Brillouin scattering involves acoustic phonons. In both cases a photon is annihilated to create another photon of lower frequency (therefore lower energy) and a phonon of appropriate momentum and energy to ensure conservation of energy and momentum. The new frequency generated by stimulated Raman and Brillouin scattering forms what is known as a Stokes wave. In single-mode fibres the Stokes wave generated by Brillouin scattering travels in the opposite direction to that of the pump whereas for Raman scattering it can travel in either direction. The shift in frequency from the pump to the Stokes wave is also much smaller in Brillouin scattering by almost three orders of magnitude.

Stimulated Raman scattering is used in Raman amplification systems where a high power pump wave is sent along with a signal wave where $\omega_{\text{pump}} >$

ω_{signal} and through Raman scattering the pump wave produces waves with the frequency of the signal wave, increasing its optical power.

In an optical fibre once the pump power has reached a threshold value then the amount of light generated in the Stokes wave can rise very rapidly. In general for longer pulses (<1 μs) Brillouin scattering has a lower threshold value than that of Raman scattering but for short pulses (<1 ns) Brillouin scattering doesn't occur at all.

Intra-pulse Raman scattering is the term used to describe when a pulse with a wide bandwidth and high power can provide its own pump and signal waves. This leads to Raman amplification of the lower frequencies of the pulse and a decrease in power of the higher frequencies. This is discussed more in section (2.7).

Four-wave mixing involves the propagation of at least two photons that are annihilated to produce two new photons each with different frequencies. If we take the case of two waves with frequencies ω_1 and ω_2 ($\omega_1 < \omega_2$) then the generated waves will have frequencies of $\omega_3 = \omega_2 - (\omega_1 - \omega_2) = 2\omega_2 - \omega_1$ and $\omega_4 = \omega_1 + (\omega_1 - \omega_2) = 2\omega_1 - \omega_2$. In order for this process to occur there must still be a conservation of energy $\omega_1 + \omega_2 = \omega_3 + \omega_4$ and the two initial waves must satisfy the phase matching condition of $\delta k = \beta_1 + \beta_2 - \beta_3 - \beta_4 = 0$ or at least keep δk to within the gain profile given by

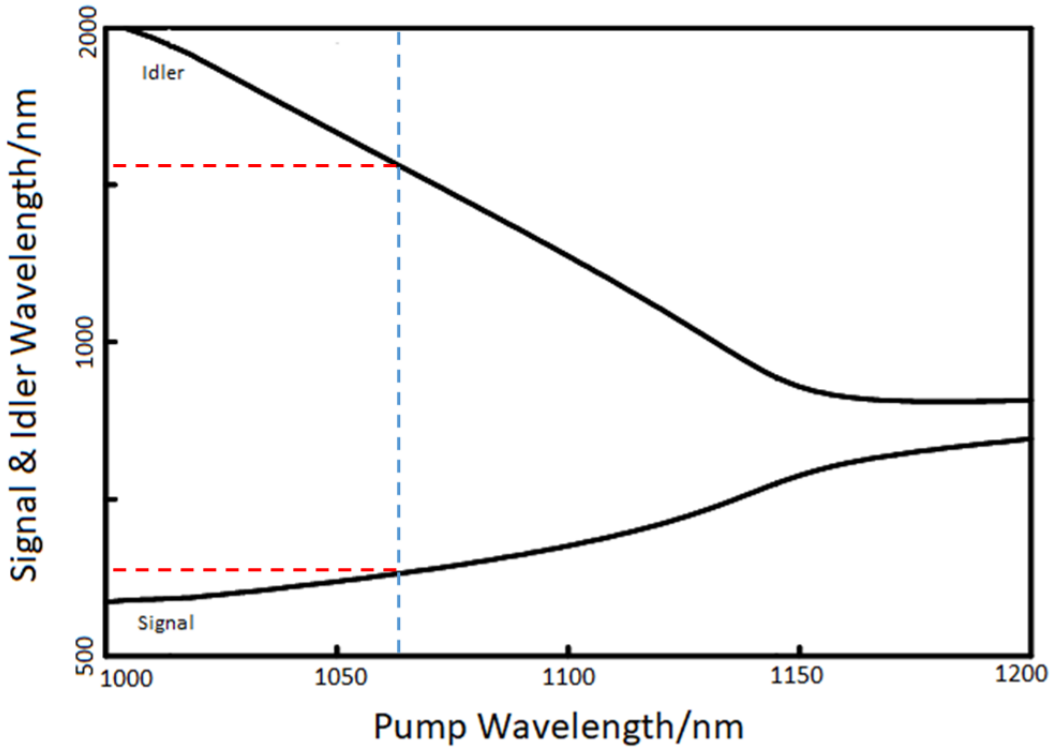

Figure 2.5 Phase matching plot for an imaginary waveguide. The lower solid line represents the phase matched signal wavelength and the upper line, the idler. The upper and lower solid lines show where the phase matched idler and signal wavelengths are for different pump wavelengths. The vertical dashed line shows a pump wavelength of 1060 nm and the horizontal dashed lines show where this pump intersects the phase matched signal and idler.

$$G(\Delta kL) = \frac{1 + \exp(-\Delta\alpha L_{ol}) - 2\exp(-\frac{1}{2}\Delta\alpha L_{ol})\cos(\Delta k L_{ol})}{\frac{1}{4}L_{ol}^2(\Delta k^2 + \frac{1}{4}\Delta\alpha^2)}, \tag{2.19}$$

where $G(\Delta kL)$ is the phase matching factor, α is the absorption coefficient, L_{ol} is the effective length of overlap of the fields (Thiel 2000).

The case of having four frequencies of light interacting through four-wave

mixing is known as non-degenerate four-wave mixing but it is possible to have four-wave mixing with a single pump source where $\omega_1 = \omega_2$. This is known as degenerate four-wave mixing and, as it must still satisfy the conservation of energy, the pump must lose 2 photons to generate the new frequencies $2\omega_1 = \omega_3 + \omega_4$. Of the two new frequencies it is common to refer to the one with the higher frequency as the signal and the lower frequency as the idler.

Phase matching plots are a common when dealing with four-wave mixing and a sketch of one is shown in figure (2.5). These plots are useful in determining where the signal and idler wavelength will be for different pumps. This phasematching plot does not represent a real fibre nor was it calculated, but it is not completely unrealistic. In figure (2.5) the vertical dashed line is set to 1060 nm and if this were a pump sent into a waveguide with this phase matching then a signal and idler would be produced at ≈600 nm and ≈1550 nm respectively. This is seen by the intersection of the pump with the phase matched signal and idler lines.

Similar to the dispersion length, there is a nonlinear length which is the distance a propagating pulse will travel in order to experience a significant amount of nonlinear effects and is defined as

$$L_{NL} = \frac{1}{\gamma P_0} \tag{2.20}$$

where P_0 is the peak power of the pulse and γ is the nonlinear parameter

defined as

$$\gamma = \frac{n_2 \omega_0}{c A_{eff}}, \tag{2.21}$$

where A_{eff} is the effective mode area and is defined as (Namihira 1994)

$$A_{eff} = \frac{2\pi[\int_0^\infty E(r)^2 \rho \mathrm{d}r]^2}{\int_0^\infty E(r)^4 \rho \mathrm{d}r}. \tag{2.22}$$

One method of increasing the nonlinearity is to decrease A_{eff} by decreasing the size of the core which requires increasing the refractive index difference between the core and the cladding of the waveguide. This confines the mode to a smaller area. This is the case for μm scale diameter silica rods, known as silica microwires. The silica acts as the core of a waveguide and the surrounding air as the cladding. This leads to a large index step and so the light is very tightly confined until the microwire's diameter falls below the wavelength of the light that it is guiding where the light begins to leak substantially into the air (Foster et al. 2008). Photonic crystal fibres with large air holes can also achieve a high level of confinement in the core through a high refractive index step (Coen et al. 2002).

2.6 The Nonlinear Schrödinger Equation

To fully describe the propagation of a wave undergoing self-phase modulation, dispersion and loss the nonlinear Schrödinger equation is needed. For relatively long pulses ($T_0 > 5$ ps) and assuming that the pulse is not propagating near to the zero dispersion wavelength the simplified nonlinear Schrödinger equation can be used (Agrawal 2000).

$$i\frac{\partial A}{\partial z} + \frac{i\alpha}{2}A - \frac{\beta_2}{2}\frac{\partial^2 A}{\partial T^2} + \gamma|A|^2 A = 0, \tag{2.23}$$

where A is the amplitude of the field envelope, and is related to losses in the fibre. The second term of equation (2.23) is related to loss in the fibre, the third contains β_2 so is related to dispersion and the last term containing γ is related to kerr noninear effects, including, four-wave mixing, self-phase modulation but not self focusing. For fibres with very low loss we can approximate $\alpha = 0$ so that the loss term can be neglected. When solving the nonlinear Schrödinger equation it is useful to express it in a normalised form and to do this, three dimensionless variables are used

$$U = \frac{A}{\sqrt{P_0}}, \tag{2.24}$$

$$\xi = \frac{z}{L_D}, \tag{2.25}$$

and

$$\tau = \frac{t}{T_0}. \tag{2.26}$$

These are then used to produce the normalised nonlinear Schrödinger equation (Akhemediev & Karlsson 1995)

$$\frac{\partial U}{\partial \xi} = -\frac{is}{2}\frac{\partial^2 U}{\partial \tau^2} + iN^2|U|^2U, \tag{2.27}$$

where $s = 1$ for normal dispersion or $s = -1$ for anomalous dispersion and

$$N = \sqrt{\frac{\gamma P_0 T_0^2}{|\beta_2|}} = \frac{L_D}{L_{NL}}. \tag{2.28}$$

The N parameter is useful for recognising soliton solutions and is discussed in more detail in section (2.7).

2.7 Solitons

Solitons are the result of a pulse where the effects of anomalous dispersion and self-phase modulation cancel each other out. To describe how this occurs we can start with the effects on the leading edge of the pulse. Self-phase modulation will induce red-shifting to longer wavelengths. These longer wavelengths will then travel slower, due to the effects of anomalous dispersion, and move towards the trailing edge of the pulse. Once these wavelengths have reached the trailing edge, self-phase modulation causes a

blue-shifting to shorter wavelengths. These shorter wavelengths will now travel faster because of the anomalous dispersion and move to the leading edge of the pulse where the process will start again. The process just described is useful in understanding the balancing act of soliton formation, but it is not accurate. Self-phase modulation and dispersion are in constant effect with the soliton remaining stationary both spectrally and temporally.

Soliton solutions to equation (2.27) are unchanging, in that there is no temporal or spectral change during propagation. For these solutions, parameter $N = 1$. Larger values of N represent higher-order solitons that do change their temporal and spectral shapes temporarily before returning over a distance known as the soliton period (Agrawal 2000, 1990)

$$z_0 = \frac{\pi}{2}\frac{T_0^2}{|\beta_2|} = \frac{\pi}{2}L_D. \tag{2.29}$$

Short pulse solitons have a large bandwidth. This can mean that the shorter wavelengths act as pumps for the longer wavelengths within the soliton. This intra-pulse Raman scattering causes a continual decrease in the mean frequency of the soliton. This is known as soliton self-frequency shift (Gordon 1986).

When a higher-order soliton undergoes intra-pulse Raman scattering it can cause the soliton to break apart into a number of fundamental solitons. This process is known as soliton fission (Dudley et al. 2006, Wai et al. 1986). It can also be caused through the effects of higher order dispersion (Sysoliatin et al.

2007). Higher-order solitons contract and then expand in the time domain over z_0 and it is at the point of maximum temporal compression that soliton fission occurs.

As a soliton propagates it can pump a higher frequency dispersive radiation in the normal dispersion regime such that

$$\beta^{\text{disp}}(\omega_{\text{disp}}) = \beta^{\text{sol}}(\omega_{\text{sol}}) \tag{2.30}$$

is satisfied, where $\beta^{\text{disp}}(\omega_{\text{disp}})$ is the propagation constant at the frequency of the dispersive radiation and $\beta^{\text{sol}}(\omega_{\text{sol}})$ is the propagation constant at the frequency of the soliton (Skryabin & Yulin 2005). This can occur if the bandwidth of the soliton is large enough to include ω_{disp}. This is far easier to achieve when the central soliton wavelength is close to the zero-dispersion wavelength. A higher-order soliton has a larger bandwidth when it has contracted temporally and so is far more likely to include ω_{disp} at this time. Similar to intra-pulse Raman scattering, the soliton acts as both seed and pump in this process. Light generated in this manner can be called a dispersive wave as, unlike the soliton, it will disperse as it propagates.

2.7.1 Supercontinuum Generation

In photonics a supercontinuum is a broadband light source that is resultant from the broadening of a laser pump. This definition is vague, as there is no

defined amount of spectral broadening that is required before a supercontinuum is formed.

The mechanisms involved in the generation of supercontinua differ depending on which dispersion regime the pump wavelength lies in. If in the normal dispersion regime then supercontinua is predominately the result of self-phase modulation and Raman. If in the anomalous dispersion regime then solitons play the leading role. All the supercontinua generated in this report have been produced using a pump that is in the anomalous regime and so these mechanics will be explained in more detail.

To start an explanation of this process let us assume a laser pump is propagating, in a fibre, very close to the zero-dispersion wavelength. The pump forms many solitons with a range of orders. The higher-order solitons expand spectrally, pumping dispersive waves that have matching ω. The dispersive waves are generated behind the solitons. The solitons continuously shift into the longer wavelengths due to soliton-self frequency shift and slow down. The dispersive waves then catch up to the solitons but cannot overtake as the solitons are raising the refractive index through the Kerr effect (Gorbach & Skryabin 2007). This is known as soliton trapping of the dispersive wave. Now the dispersive waves and solitons are travelling together and, through a four-wave mixing mechanism between the two, the dispersive waves shift into shorter wavelengths and slow down. The solitons

continue to soliton-self frequency shift, slow down and the dispersive waves catch up to start the process again. It is through this soliton trapping that the longest and shortest wavelengths of the supercontinuum are generated.

2.7.2 Manipulation of the Zero Dispersion Wavelength

For the processes discussed in section (2.7.1) to occur it is required that the laser pump wavelength be in the anomalous dispersion regime, in order to form solitons. Pumping light into the dispersive wave is more efficient the closer the wavelengths of the dispersive wave and pump wavelengths are, which is the case when the laser pump is closer to the zero dispersion wavelength. The supercontinuum work in this thesis utilises a laser pump with a wavelength of 1064 nm and as such a waveguide is needed that has a zero dispersion wavelength close to and below this wavelength as well as having this wavelength within the anomalous dispersion regime.

Fabricating an optical fibre that has these characteristics can be done by changing either the material or waveguide dispersion. Silica glass is the primary contributor to the material dispersion of typical optical fibres (dopants such as germanium and flourine do contribute but not nearly as much) and these fibres will be used in this thesis. The group velocity dispersion of silica glass is shown in figure (2.6) as the solid grey line. If a 1064 nm pump was sent into this dispersion profile it would be in the normal dispersion regime and would not form solitons. Therefore the waveguide

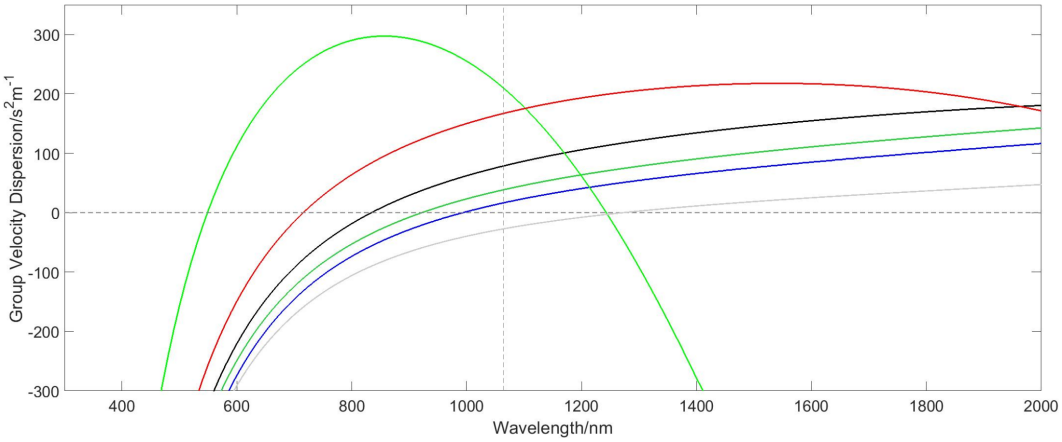

Figure 2.6 Group velocity dispersion curves for bulk silica (grey line) and silica microwires of varying diameter of varying diameter. Light Green: 1 µm. Red: 2 µm. Black: 3 µm. Dark Green: 4 µm. Blue: 5 µm. The vertical dashed line is at 1064 nm. The horizontal dashed line is set to zero on the y-axis to aid identification of zero dispersion wavelengths.

dispersion must be altered to lower the zero dispersion wavelength.

Lowering the zero dispersion wavelength can be achieved by decreasing the core diameter of a fibre whilst increasing the refractive index difference between the core and cladding. Tapering optical fibres to a diameter of only a couple of micrometers achieves this as the strand of glass acts as a fibre core and the cladding is the surrounding air. Figure (2.6) shows the group velocity dispersion for several microwires of varying diameter. As the diameter gets smaller the zero dispersion wavelength decreases, allowing the 1064 nm pump to now form solitons that are close to the zero dispersion wavelength.

It can be seen in figure (2.6) that when the diameter is 1 µm (light green line), a second zero dispersion wavelength becomes visible just below

1300 nm. This second zero dispersion wavelength would significantly affect any supercontinuum generation. The affect of this second zero dispersion wavelength will not be investigated in this thesis but it's utilisation is of interest in the field to tailor the spectral shape of supercontinuum (Raj et al. 2015, Frosz et al. 2005).

Chapter 3

Supercontinuum Generation using Tapered Optical Fibres

Using tapered optical fibres to generate supercontinuum has been done before due to the ease with which the zero-dispersion wavelength can be adjusted by choosing the taper waist diameter (Foster et al. 2004, Tong et al. 2004). For example a supercontinuum spanning 370 - 1545 nm was made by using 100 fs pulses in a taper with a 2 μm diameter and a length of 90 mm (Birks et al. 2000). Tapers with a diameter of less than a micron have also been used with femtosecond pulses to generate supercontinuum (Leon-Saval et al. 2004, Foster et al. 2005). Another example is a 5.6 W picosecond white light source that was made by splicing tapered fibres to one another (Teipel et al. 2005).

3.1 Tapering

There are several ways to taper a fibre into a silica microwire but the basic principle involves heating the fibre, to soften the glass, whilst simultaneously pulling along its length so that the heated region is stretched to a smaller diameter. The source of heat can be a ceramic microheater, (Wang et al. 2012, Ding et al. 2010) an electric arc (Shao et al. 2013), a naked flame, (Burns et al. 1985, Witkowska et al. 2006) and more as long as it is sufficient to heat the fibre so that it is able to be stretched without breaking (Yokota et al. 1997, Dimmick et al. 1999).

Fibre tapering is often a specific process that requires unique combinations of equipment. Wang et al. (2018) constructed a tapering rig from scratch due to their need to taper a non-oxide glass with a narrow temperature range of appropriate viscosity. An aluminium heating block with a heat zone of 4 mm was used and the fibre pulled by stages that had to be activated manually. The temperature was raised slowly until the fibre was seen to 'sag' at which time the stages were activated to stretch the fibre.

Tapering fibres has other uses than for supercontinuum generation. Two fibres placed closely together in parallel will form a fibre coupler if tapered down (Wilson et al. 1975). If a fibre is tapered enough then a significant amount of evanescent field will be outside of the glass which can be used in sensing for pressure (Bariain et al. 2000), temperature (Datta et al. 1996)

chemical sensing and more (Henry 1994).

The method used in this report is the flame brush technique where the fibre is placed between two stages that pull in opposite directions whilst a flame moves up and down the length of the fibre as shown in figure (3.1). Parts of the fibre that are heated then become thinner as it is stretched. The process is run through a computer where the desired taper shape is programmed in. The human component involves stripping the fibre of coating, strapping the fibre to the two stages, lighting the flame, placing the flame underneath the fibre and removing it once the program has run its course.

This method allows the creation of a narrow waist with unstretched fibre to either side connected via two transition regions (Birks & Li 1992). By careful management of the burner speed and position, it is also possible to create tapers of more complex design with inner-waist transitions connecting taper waists of different diameters. It is important when tapering fibres to ensure that each of the transition regions is gradual enough to prevent high losses.

As discussed in section (2.3) waveguide modes depend upon the transverse geometry of the fibre and so in a transition region of a taper the transverse geometry is constantly changing along the direction of propagation. The propagating mode can change and continue to propagate if the rate of change is slow enough. If the rate of change is too high then it will cause loss. If a transition is low loss then it is known as adiabatic (Love et al. 1991).

a)

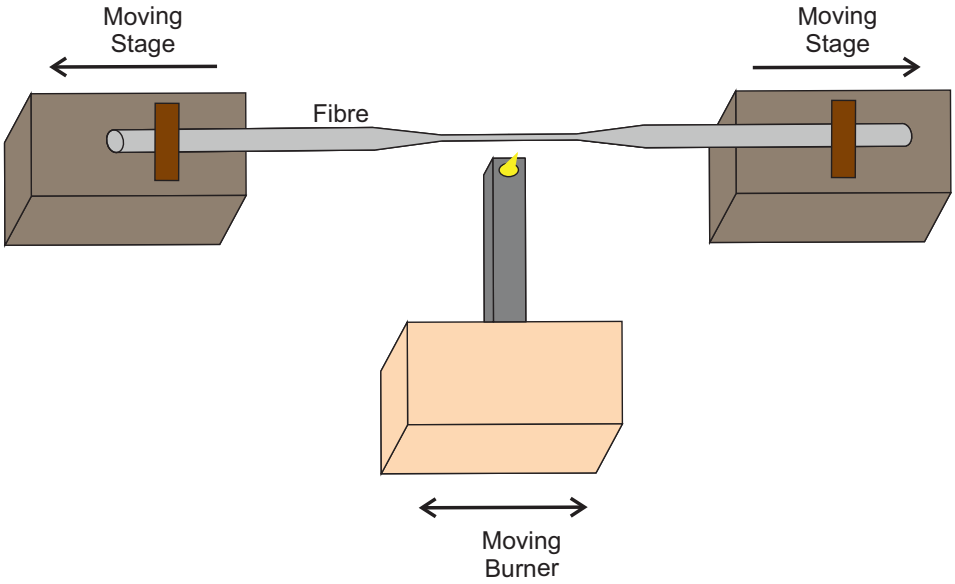

b)

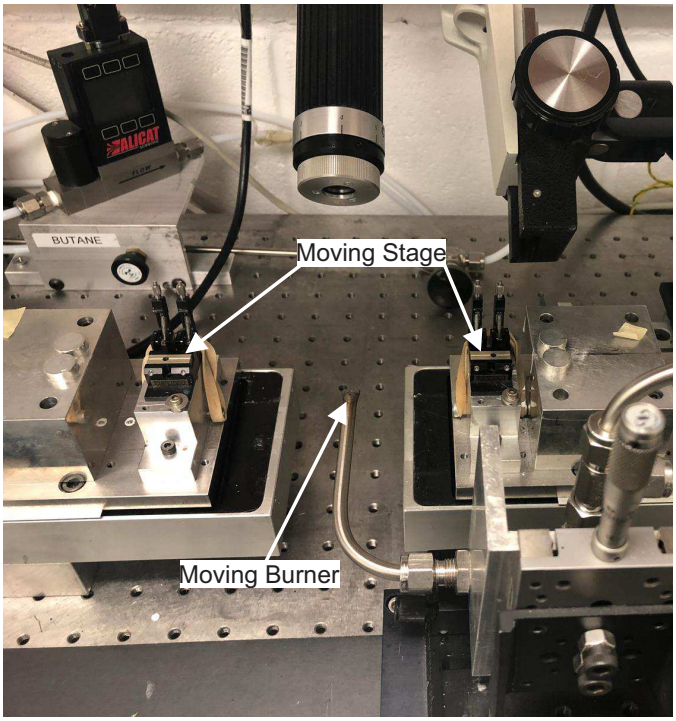

Figure 3.1 (a) Diagram of taper rig showing the burner that heats the fibre as the stages move apart to stretch the fibre into a taper. (b) Photo of the taper rig with labels for the stages and burner

Early on in this project a taper was made that had a final diameter of 1 μm. This taper was made by stretching a standard telecommunication fibre SMF-28 that has a cladding diameter of 125 μm. SMF-28 is a very common commercial fibre that is used in telecommunication. The 1 μm taper was place on a microscope slide. A length of untapered SMF-28 was then placed perpendicularly on top of the 1 μm taper. The slide was placed underneath an optical microscope. Figure (3.2) shows an image taken through this microscope at a magnification of 20×. The focus of the microscope is on the 1 μm taper and so the untapered SMF-28 is blurry due to being out of focus. This image is not sufficient to measure the diameter of the tapered fibre. If the procedure for tapering fibre is followed and there is no slippage of the fibre from the clamps then, due to its function being based upon the conservation of volume, the final taper must be close to the desired diameter. The measured properties are reproducible confirming the precision of the diameter. The absolute size may be different from predicted as the flame has some width, not the zero width assumed in the model.

3.2 Uniform Tapers

3.2.1 Introduction

In the following section tapers with uniform waist diameters and varying lengths up to 250 mm were made and tested. This was done to see if tapers

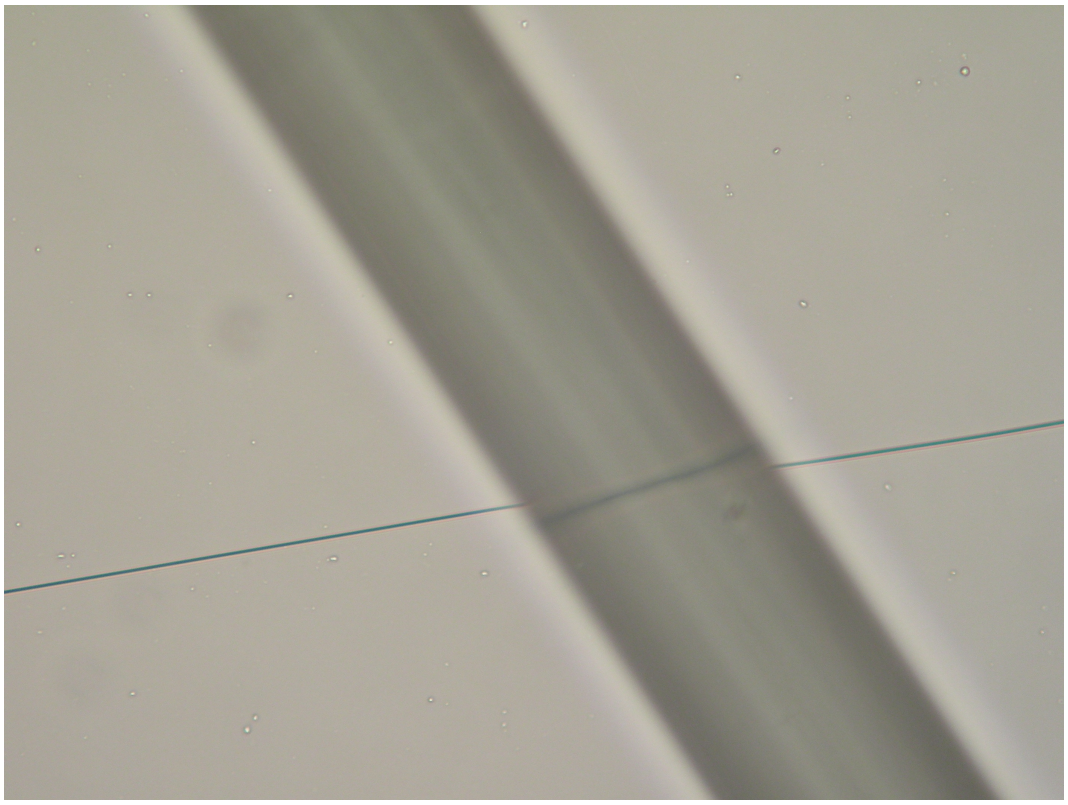

Figure 3.2 Photograph taken through a microscope set to a magnification of 20×. The thick structure passing through the top and bottom of the image is a length of SMF-28 optical fibre. The thin horizontal line is a length of SMF-28 that has been tapered down to a diameter of 1 µm and placed beneath the untapered SMF-28. The microscope is focussed to the 1 µm taper and so the untapered SMF-28 is out of focus and appears blurry.

of this length could be fabricated at sufficiently thin diameters to produce supercontinuum, using the setup shown in figure (3.4). Investigating the effect of taper waist length on the generated supercontinuum was also explored.

A diagram of a typical taper is shown in figure (3.3). The dashed transition regions are not shown to scale with the rest of the diagram as they are long

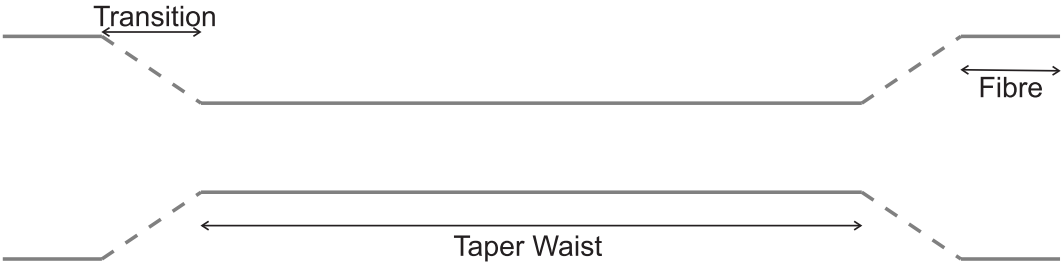

Figure 3.3 Diagram of a taper with labels showing different sections. The transitions are typically around 40 mm in length. The taper waist can be up to 250 mm

and relatively uninteresting, beyond the requirement for being adiabatic.

3.2.2 Experimental Setup

A diagram of the experimental setup is shown in figure (3.4). A Fianium FP-1060-20-PP laser source was used to emit 5 ps pulses, that are not transform limited with a repetition rate of 1 MHz. A schematic of the laser is shown in figure (3.5) From the laser, two mirrors and a 30x aspheric lens were used to couple into the SM980 fibre. A half-wave plate and polarising beam splitter were used to control the power reaching the fibre. The optical spectrum analyser used was an ANDO AQ 6315B which can be used for wavelengths between 350-1750 nm and was set to a resolution of 5 nm. An OPHIR 3A-FS-SH thermal power meter was used to measure the power. This was done at the output of the fibre and just before the beam enters the lens. The SM980 fibre has a similar design to SMF28 except it has a smaller core (4.5 μm) designed to lower the cut-off frequency to 980 nm which helps

to reduce the concentration of higher order modes. The SM980 has also been manufactured with a reduced cladding diameter of 80 μm which makes the taper transitions easier to make adiabatic.

The supercontinuum tapers are suspended between two towers connected via a metal bridge. The full size fibres, either side of the taper, are stuck to the towers using tape with the taper suspended in air between them. All of this is then placed within a plastic cylinder with caps on the end that had small holes to allow the fibre to be fed out of either end. The towers and bridge kept the taper straight and prevented any movement of the fibre that could damage the taper. The plastic cylinder isolated the taper, helping to stop air currents, dust particles and accidental physical contact that could damage the taper.

It is key to understand the importance of protecting the taper from damage. When a fibre has been tapered down to a diameter of only a few micrometers it becomes very delicate. If not kept taut then the taper can be severely damaged by relatively light air currents such as someone breathing. This usually leads to the taper snapping at a point along the transitions connected to the full size fibre. Dust is also a problem in that it is now of comparable size to the taper waist. This is not a structural problem, as the dust is not that heavy in comparison to the taper waist, but the evanescent field extends into the air or whatever happens to be touching the waist. This leads to increased loss and also heats the dust creating a weak point on the taper. Figure (3.6)

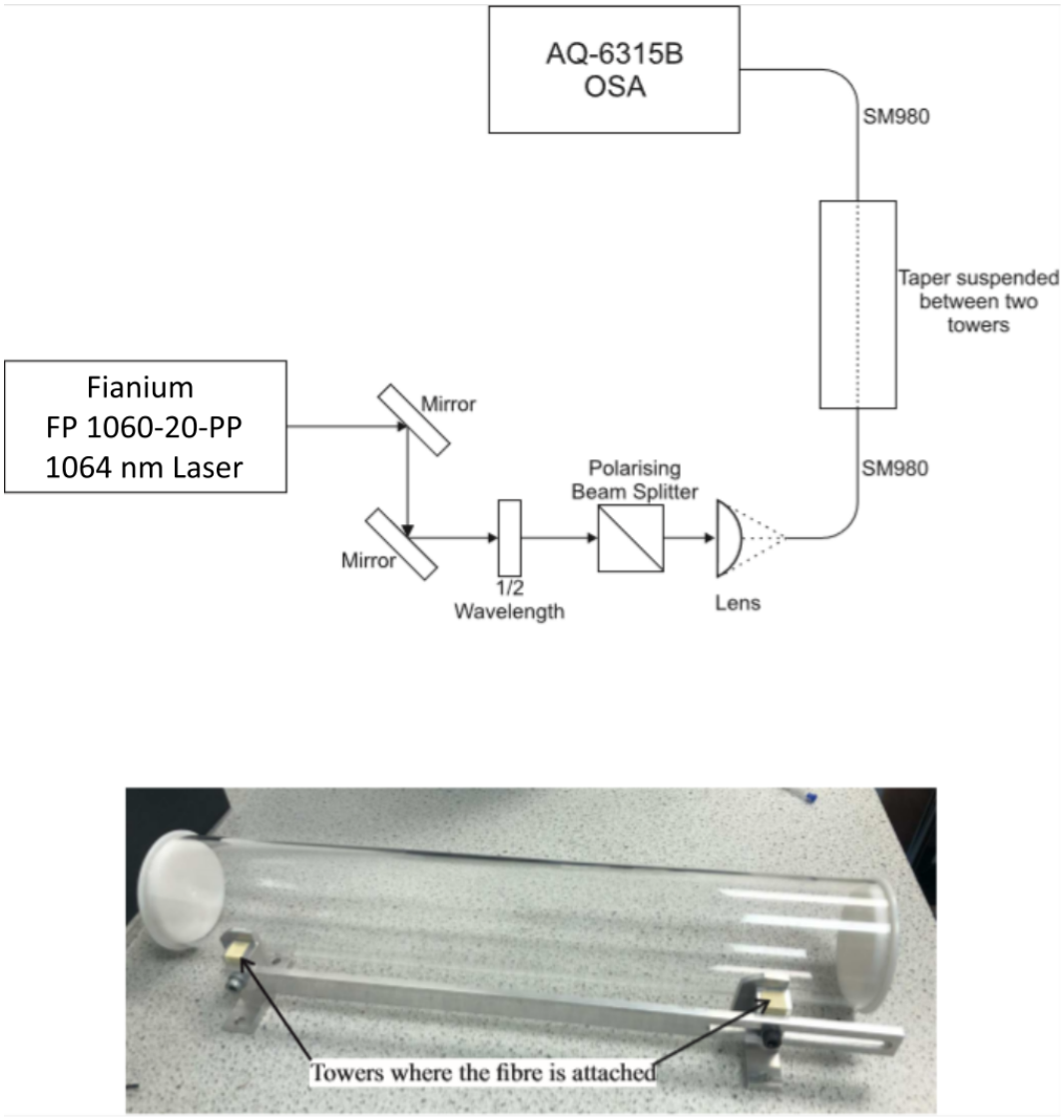

Figure 3.4 Setup used for taking spectra from supercontinuum tapers. A photo shows the two towers used to hold the tapers. The full diameter fibre at either end of the taper is held by the two yellow tapes. This is then placed within the plastic tube behind it in order to protect it from damage. Either end of the plastic tube has a small hole to allow the fibre to be fed through.

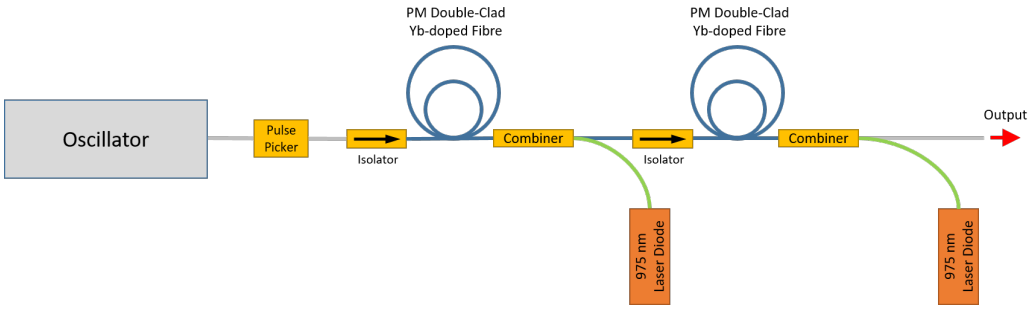

Figure 3.5 Schematic of FP 1060-20-PP laser shown in figure (3.4).

shows a photo taken through an infrared viewer of a taper that has several dust particles one of which is circled. To reduce this problem a high efficiency particulate air filter was run for several hours before the tapering process and constantly until the taper was placed safely within the plastic tube.

Because the input and output fibres are always the same type, with different taper designs, the output spectra can be quantitatively compared as the input coupling and spectrometer coupling are always the same. This is very beneficial for analysis compared to supercontinuum in photonic crystal fibres where the coupling, and the dependence of coupling on wavelength, will change if the fibre core design is altered.

3.2.3 A note on supercontinuum results

Supercontinuum generating tapers were made and investigated over the course of three years of this PhD. The vast majority of the results in this thesis however were taken in the last year of the three. Towards the end of the second

Figure 3.6 Photo taken, through an infrared viewer, of a taper generating supercontinuum. Dust can be seen as bright spots, one of which is circled.

year of study the laser system used to pump the tapers broke. It was sent to the manufacturer, repaired and returned. Upon return the laser performed differently than in the previous two years with improved beam quality, slightly shorter pulses and narrower bandwidth. The laser system was not new and was most likely undergoing a slow decline in performance before it was noticed, with the repair revealing the normal state of operation. This means that the results taken after the laser was repaired are not comparable with those taken before.

A notable difference can be seen when comparing spectra from supercontinuum generating tapers from before and after the repair. Figure (3.7) shows spectra from a taper that has been pumped by the laser before and after the repair. It can be seen that after the repair a lower amount of average power is required to attain a supercontinuum of similar

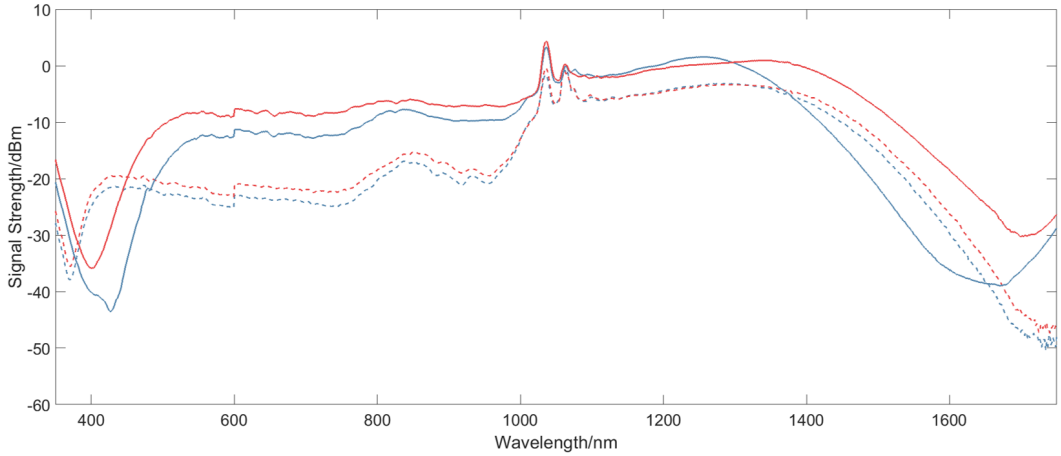

Figure 3.7 Spectra taken from two tapers with the same design. The solid lines were taken before the pump laser was repaired with blue at 100 mW and red at 125 mW output power. The dashed lines were taken after the laser was repaired at output powers of 60 mW for blue and 70 mW for red.

spectral width.

A higher peak power would result in a shorter nonlinear length (2.20) and the nonlinear processes involved in the generation of a supercontinuum occurring over a shorter length. Peak power is proportional to average power and inversely proportional to pulse width. If the repaired laser pulses are shorter than they were beforehand then we should see similar amounts of nonlinear processes occurring at lower average powers which is seen in figure (3.7). This is one possible explanation for the differences seen but it is likely to be a combination of factors.

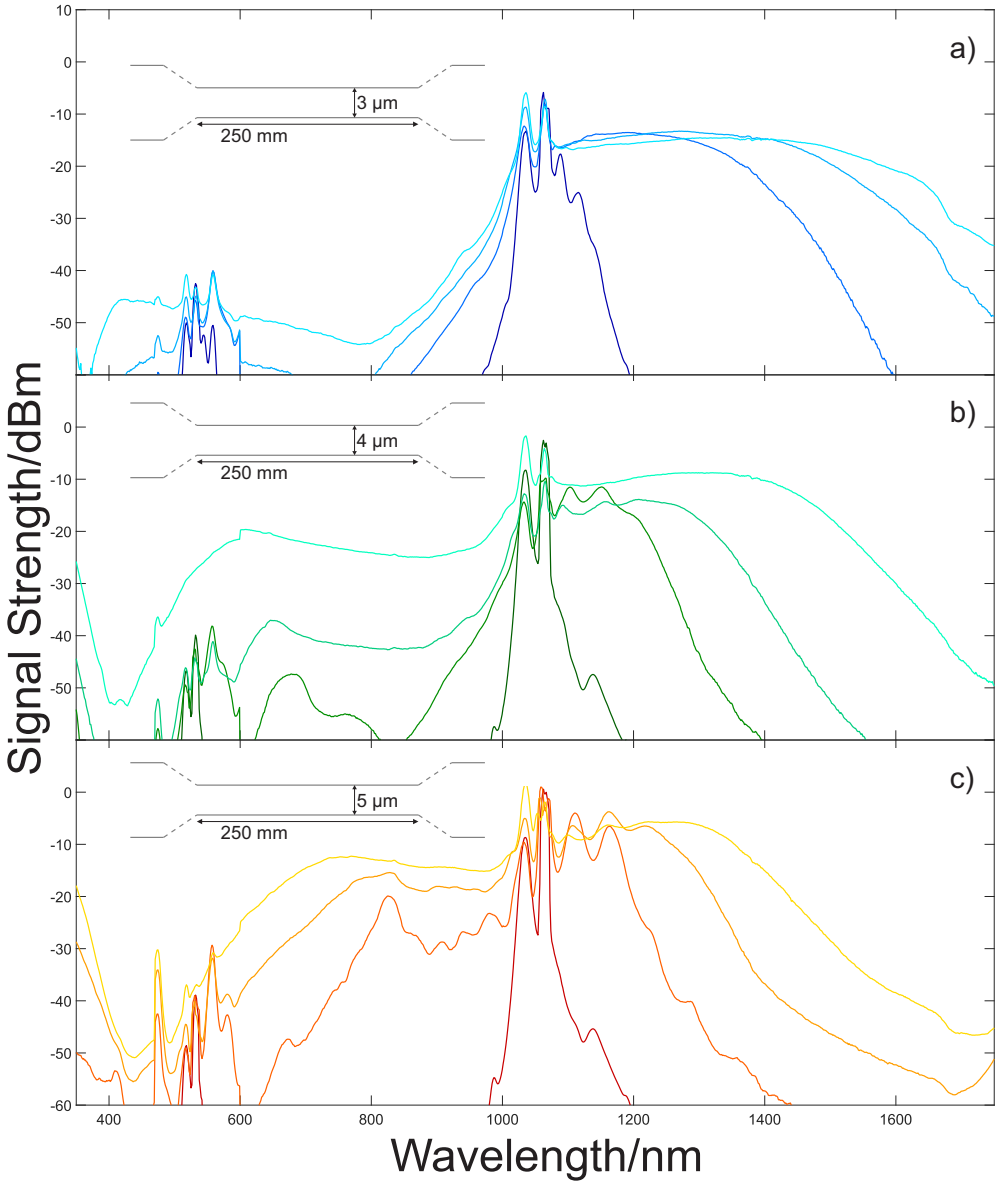

Figure 3.8 Spectra from three tapers, with different taper waist diameters. (a) 3 µm diameter waist (b) 4 µm diameter waist (c) 5 µm diameter waist. All tapers had a waist length of 250 mm. (a), (b) and (c) all show output powers of 10, 20, 50 and 70 mW, starting from the narrowest to broadest trace of each taper.

3.2.4 Results

In figure (3.8) three sets of spectra are shown with similar output powers. In figure (3.8 c) the red line has the narrowest spectrum with little broadening due to it having the lowest power. At the next power (dark orange) it is much broader, reaching ≈800 nm into the short wavelengths and ≈1250 nm into the long before dipping below -30 dBm. The longer wavelengths are predominately being generated by soliton self-frequency shifting and the shorter wavelengths by dispersive waves. Both processes are described in section (2.7). The dispersive wave first appears at ≈850 nm at the second lowest power (dark orange). As the output power increases in the light orange and the yellow traces shorter and longer wavelengths are generated broadening the spectrum. This is evidence of soliton trapping. The soliton, created around 1064 nm, self-frequency shifts into the longer wavelengths and the dispersive wave is trapped maintaining the same group velocity causing it to move into ever decreasing wavelengths.

The same process of soliton trapping can be seen in figure (b) but not in (a).(a) does reach the longest wavelengths when compared to the others which means there is a greater amount of soliton self-frequency shifting but the zero dispersion wavelength is too low for generation of a dispersive wave until higher powers. The purpose of this experiment was to get the broadest and flattest supercontinuum so the 3 μm diameter taper is clearly unsuitable as it does

not generate short wavelengths in sufficient enough power. Taking the highest output powers of the remaining tapers and observing where their spectra dip below -30 dBm, the 5 μm diameter taper spans between ≈560 - 1520 nm and the 4 μm ≈500 - 1600 nm.

The peaks between 400 - 600 nm that appear in all three spectra (and every spectrum in the section) are most likely a combination of multimodal four-wave mixing and artefacts from the order sorting of the optical spectrum analyser. The peaks towards 600 nm certainly are caused by order sorting as there is a sudden drop where the optical spectrum analyser switches order. It is not the purpose of this experiment to generate sharp peaks at low power and so they will not be considered worthy of note. The optical spectrum analyser changes detectors at 600 nm and this can be seen as a small discrete step in some spectra. This step is small and does not hinder analysis of the spectrum. At the edges of the optical spectrum analysers range, gain errors can be seen. These errors are because the gain factors are very large due the detectors being less sensitive. Taking the highest power in figure (3.8) (c) it can be seen that the optical power drops from 780 nm to 450 nm and then rises again. This rise is unlikely to be "real" light as the optical power is clearly dropping from the dispersive wave. These gain factor errors are apparent and should be ignored when analysing the spectra.

To investigate the effect of taper waist length, tapers with the same waist

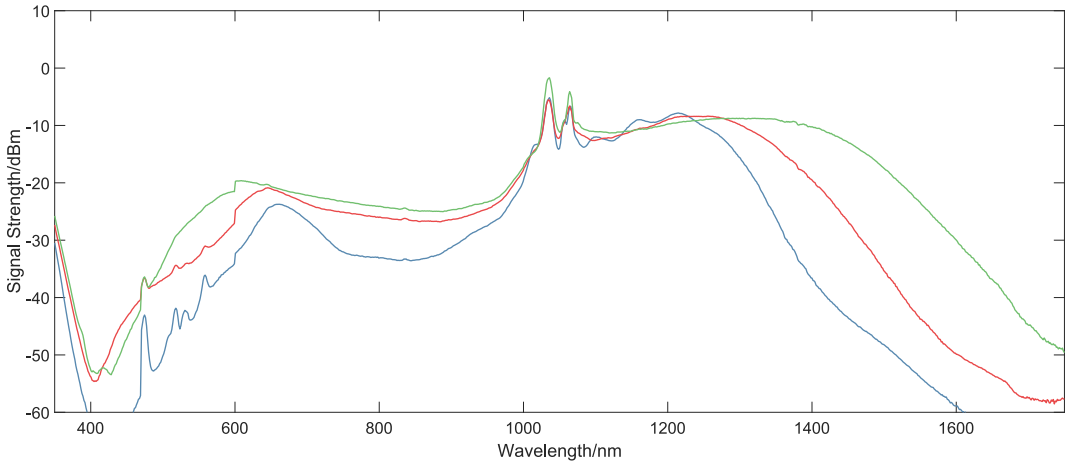

Figure 3.9 Spectra of three tapers, all with the same taper waist diameter of 4 μm and output power of 70 mW but different waist lengths. Blue: 150 mm Red: 200 mm Green: 250 mm

diameter and different lengths were made to compare the supercontinua they generated. The tapers from figure (3.9) all have a taper waist diameter of 4 μm. The reason that this taper waist diameter was chosen can be explained by looking again at figure (3.8). It was important that the chosen taper waist diameter be capable of generating a wide supercontinuum of decent optical power. The 3 μm taper couldn't generate a supercontinuum with meaningful power. Both the 5 and 4 μm tapers generated supercontinua but the 4 μm had a wider bandwidth. The width was important as any differences from waist length would be easier to identify.

Figure (3.9) shows the spectra from 3 tapers of the same waist diameter but different lengths at the same output powers. The question of whether length helps to generate a broad supercontinuum is answered here by the longest waist

reaching the lowest and highest wavelengths whilst also having the flattest spectrum. The difference between the 250 mm taper and the 150 mm in terms of spectral width is the 250 mm taper reaching ≈130 nm further into the short wavelengths and ≈220 nm in the long wavelengths. The most notable negative for using longer waist tapers is that they are more susceptible to damage. They are also harder to taper successfully as the tapering process takes more time and if something is wrong, such as the stages being out of alignment, then the process is more likely to fail.

3.2.5 Conclusions

The results in figure (3.8) show that tapers of μm scale can be made and produce supercontinuum through soliton fission. These supercontinuum can span over 1000 nm, whilst maintaining a power over -30 dBm, when place in the setup shown in figure (3.4). Decreasing the diameter of the taper waist does lower the power level reached by the dispersive wave and at very low diameters the dispersive wave is not generated with significant power.

Figure (3.9) shows that increasing the length of the taper waist increases the width of the spectrum and the power in the long and short wavelengths. The only drawback being the fragility of long tapers.

3.3 Non-uniform Tapers

3.3.1 Introduction

Producing novel ultraviolet light sources is of current scientific interest for their uses in spectroscopy, photochemistry and more (Yu et al. 2018, Abramov et al. 2018). A popular approaches in photonics is to use supercontinuum generation. Gao et al. (2014) published a paper using a giant-chirped mode-locked Yb-doped fibre laser as a pump for a uniform photonic crystal fibre to generate supercontinuum ranging from 370 - 2400 nm. Belli et al. (2015) reported the generation of a supercontinuum spanning 124 - 1200 nm using a hydrogen filled PCF pumped with 30 fs pulses at 805 nm. Both of these papers emphasise the ultraviolet end of the spectrum as a 'selling point' of their discovery. These papers are not unique for this (Joly et al. 2011, Kudlinski et al. 2006, Jiang et al. 2015).

The experimental setup used in this report is relatively simple/cheap (especially the 1064 nm MOPA pump laser) in comparison to others (Ermolov et al. 2015, Hosseini et al. 2018). If it is possible to produce ultraviolet wavelengths (with reasonable power) then that could provide a cost effective ultraviolet light sources.

In order to produce light at shorter wavelengths the diameter of the taper must be small enough to shift the zero dispersion wavelength away from the pump. Figure (3.8) (a) shows that, at smaller taper diameters, a larger amount

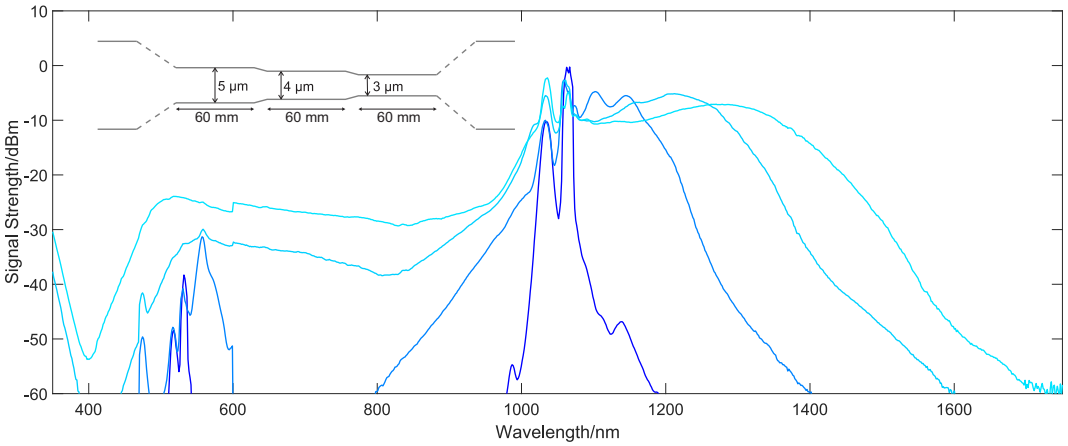

Figure 3.10 Spectra taken from a taper with three different waist diameters of 5 µm, 4µm and 3µm each with a length of 60 mm. Transitions connecting these waists are 10 mm in length. Output powers are 10, 20, 50 and 70 mW, starting from the narrowest to broadest trace.

of input power is needed to produce a dispersive wave with comparable optical power to the rest of the spectrum. The aim of this section is to generate light at as short a wavelength as possible without the need for high pump powers.

The tapers in this section are formed of stages that decrease in diameter. This will allow dispersive waves to be produced in the first taper waist that will become trapped by solitons. Decreasing the taper diameter once this has occurred will force the trapped dispersive wave to be pushed to shorter wavelengths as the soliton decelerates faster in the high group velocity of the smaller taper. This allows the generation of a dispersive wave with a significant amount of optical power before broadening is induced to shorter wavelengths.

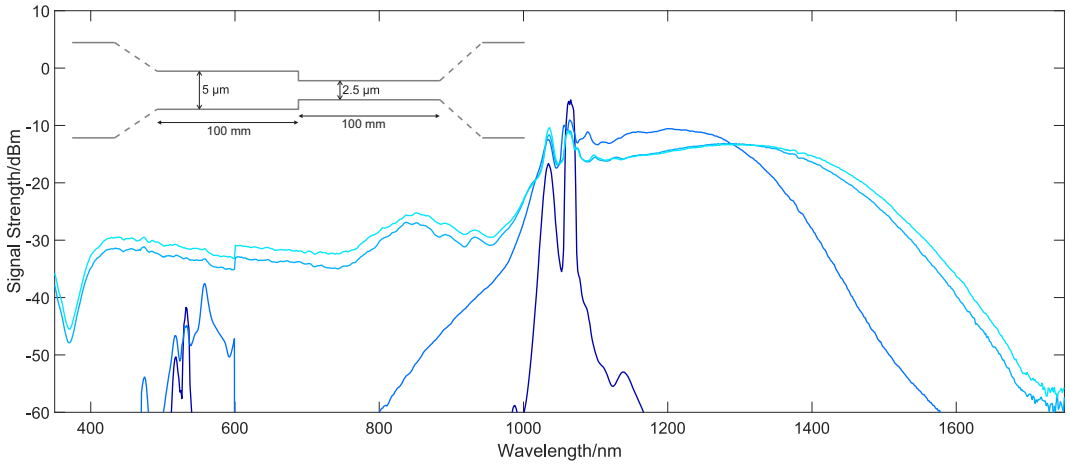

Figure 3.11 Spectra taken from a taper with two waist diameters of 5 µm and 2.5 µm. Both diameters are 100 mm in length. The transition between the two waist diameters was sharp as possible. Output powers are 10, 20, 50 and 70 mW, starting from the narrowest to broadest trace.

3.3.2 Results

Figure (3.10) shows the spectra taken from a taper witch starts at 5 µm and then transitions to 4 µm and finally 3 µm. This design gave spectra which extended further into the shorter wavelengths than the uniform tapers shown in section (3.2) and reached 480 nm. The long wavelength side only extends to ≈1500 nm. It was expected that this design would not increase the broadening into the long wavelengths when compared to 3 or even 4 µm uniform tapers as the sections are not very long. It is surprising that the long wavelength is beaten by the 5 µm uniform taper as this design starts at that size and then goes even smaller.

The design of taper used in figure (3.11) was to test to see if the soliton trapping of dispersive waves could be broken. The initial 5 µm section will

produce a dispersive wave but the transition into the 2.5 μm section was made as sharp as possible. It should be noted that the transition would not be a completely discrete step, as shown in the diagram, but is more likely to be a transition of the order of a few millimetres as this is limited by the width of flame used in the tapering process. The sudden change in dispersion could cause the solitons to lose their dispersive waves. The second section of the taper waist is 2.5 μm in diameter which has not been shown before. This diameter was used in other designs before this similar to the one shown in figure (3.10) and was found to work effectively.

The spectrum produced is very broad spanning 420 - 1550 nm. This shows that at least some of the dispersive waves have remained trapped or have escaped their soliton and been re-trapped by another soliton. This provides evidence that the trapping effect is strong enough to handle inner-waist transitions which are tens of millimetres long.

Tapers were made to ascertain what ratio of lengths of 5 μm to 2.5 μm would give the shortest wavelength through supercontinuum generation. To investigate this, many tapers were made all starting with a 5 μm section followed by a 2.5 μm section. These tapers were limited to a maximum waist length of 200 mm including the transition between the 5 μm and 2.5 μm sections, which is 20 mm in length. Figure (3.12) shows spectra from four of these tapers.

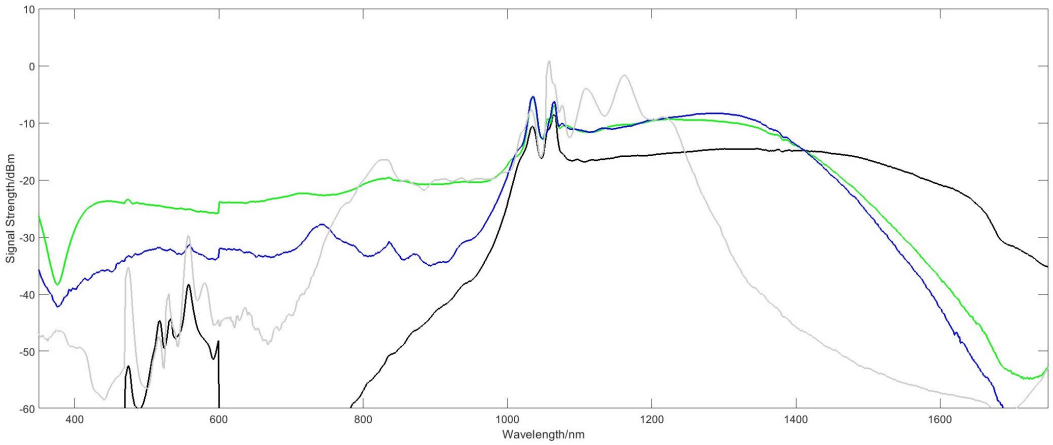

Figure 3.12 Spectra taken from 4 different tapers that each begin with a 5 µm diameter section followed by 2.5 µm diameter. The length of these two sections is different for each taper. The output power for each is 70 mW. Black: 40 mm length of 5 µm followed by 140 mm of 2.5 µm. Blue: 90 mm length of 5 µm followed by 90 mm of 2.5 µm. Green: 140 mm length of 5 µm followed by 40 mm of 2.5 µm. Grey: 170 mm length of 5 µm followed by 10 mm of 2.5 µm.

The taper that has the shortest length of 5 µm diameter (shown in black) does not generate significant power in the shorter wavelengths, through a dispersive wave, but does reach furthest into the longer wavelengths out of the three. The lack of dispersive waves is due to the an insufficient length of 5 µm diameter whereas the reach into the longer wavelengths is from the long length of 2.5 µm causing increased soliton self-frequency shift.

The taper with a 10 mm section of 2.5 µm diameter (shown in grey) doesn't reach as far into the long wavelengths as the others and doesn't generate more than -30 dbm below $\approx$ 740 nm. The lack of long wavelengths is due to reduced soliton self-frequency shift. It is clear that a dispersive wave has been generated just above $\approx$800 nm and, as this matches the wavelength of the dispersive wave

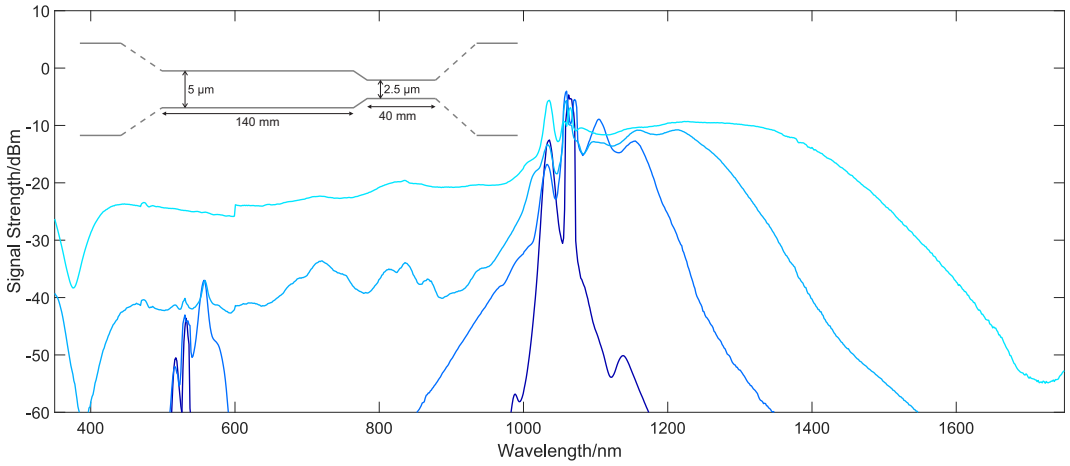

Figure 3.13 Spectra taken from a taper with two waist diameters of 5 and 2.5 µm. The waist with diameter of 5 µm has a length of 140 mm. The waist with diameter of 2.5 µm has a length of 40mm. The transition connecting the two different diameter waists has a length of 20 mm. Output powers are 10, 20, 50 and 70 mW, starting from the narrowest to broadest trace.

seen in figure (3.9) (c), it is generated in the 5 µm section, with the 2.5 µm section having little to no effect.

The remaining two (blue and green) spectra are similar in how far they reach into the longer wavelengths but the taper with a 90 mm length of 5 µm diameter has lower power for all of the wavelengths shorter than 900 nm. It was decided that the taper that produced the spectra shown in green was the best for producing short wavelengths and maintained a power above -30 dbm for a range of 420 - 1550 nm.

In figure (3.13) shows two peaks at wavelengths of 715 and 820 nm in the spectrum with the second highest power level. The peak at 820 nm matches the wavelength of the dispersive wave seen in figure (3.8) (c) and shows that

soliton fission has occurred in the 5 μm section of the taper. This dispersive wave has then been dragged into the shorter wavelengths by the 2.5 μm section of the taper. The peak at 715 μm could have been generated at the same time as the one at 820 μm and become seperated by the dip appearing just below 800 μm. This dip is at the zero dispersion wavelength of a 2.5 μm taper waist which means that light at wavelengths higher than this would form solitons and shift to longer wavelengths whilst shorter wavelengths are dragged to shorter wavelengths through soliton trapping. The net effect would be a loss of light at the zero dispersion wavelength.

Figure (3.14) is a photograph of a screen where the output fibre from the taper that produced the spectra in figure (3.13) is being held in front of it. The photo was taken using a smart phone. The fibre was held approximately 20 cm from the screen and was held such that the fibre was directly incident on the flat screen. The output power is 70 mW which corresponds to the highest power shown in figure (3.13). The output is circular with a centre that is white. This white centre arises as light of all visible wavelengths is present. It is expected to be white as the spectra in figure (3.13) shows that there is detectable light at all wavelengths in the visible spectrum. Moving from the centre of the circle outwards it can be seen that the colour changes. This change goes from white to having a red hew to blue at the edges. The centre is white where all the wavelengths are present, the change to red is from those

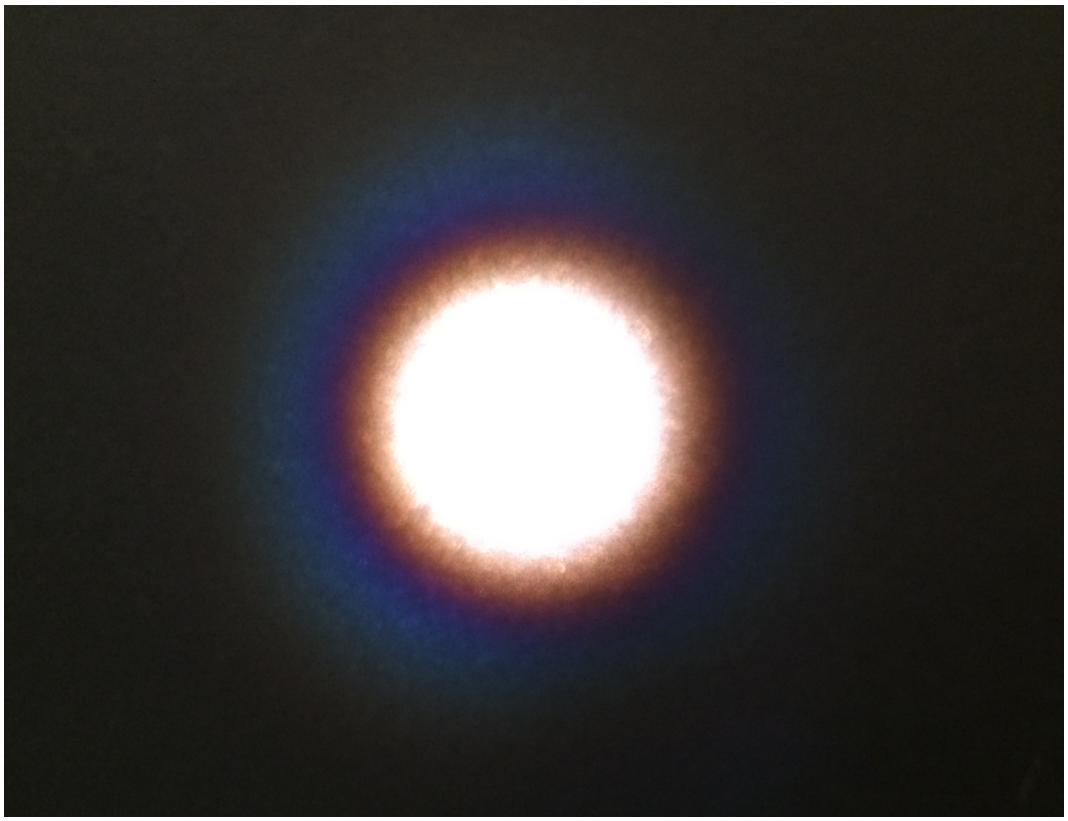

Figure 3.14 Photograph of the output from taper whose spectra is shown in figure (3.13). The output fibre was held 20 cm from a screen in a dark room. This was taken using a smart-phone camera.

longer wavelengths diffracting more once leaving the fibre. The blue outer ring is most likely from a higher order mode that then has a numerical aperture.

3.3.3 Conclusions

Using a taper consisting of a 5 μm diameter section of 140 mm length followed by a 2.5 μm section of 40 mm length allowed the generation of a dispersive wave that remained trapped by solitons to produce a supercontinuum with an optical power above -30 dBm in a range of 420 - 1550 nm.

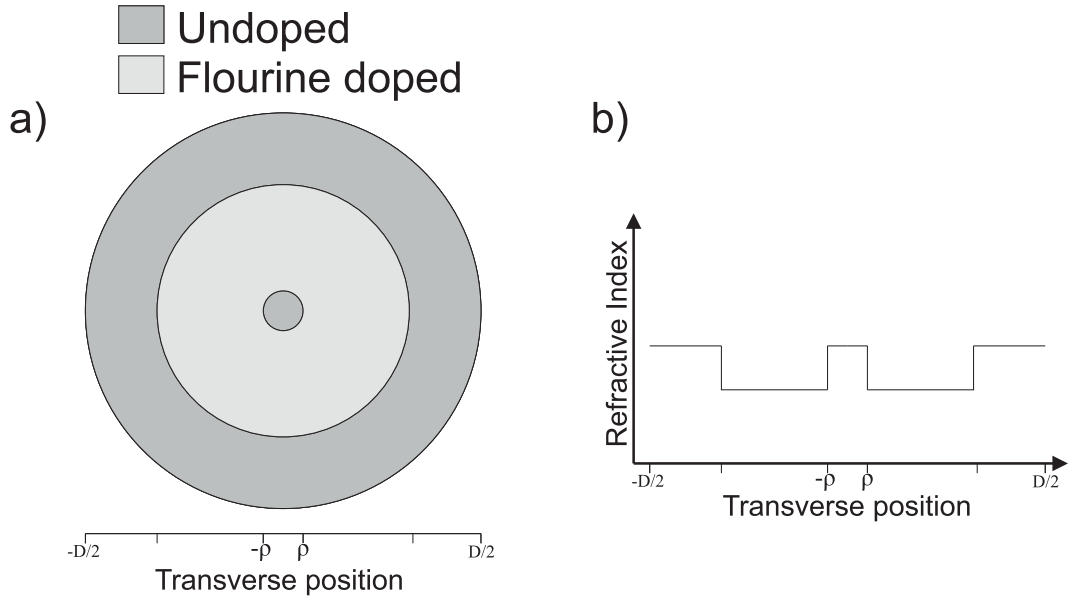

Figure 3.15 (a) Transverse diagram of a typical fibre that has part of the cladding doped with fluorine. (b) Transverse refractive index profile of (a). ρ is the core radius and D is the cladding diameter.

By using a non-uniform taper waist that decreases in diameter along the direction of light propagation it is possible to shift an already generated dispersive wave into the short wavelengths. Uniform tapers would require higher input power to generate a dispersive wave (of comparable spectral power) at wavelengths so short.

3.4 Germanium-free Fibres for the UV

3.4.1 Introduction

To reach wavelengths that are lower than those reached by figure (3.13) absorption by germanium becomes a problem. Germanium has a strong

absorption peak at 380 nm and is a common dopant in the core of optical fibres, in order to raise the refractive index above the cladding. Fluorine doped cladding is a common alternative to achieve the required index step with a pure silica core but it is usually not doped uniformly throughout. For example part of the cladding may be doped starting from the inner edge. This forms a trench when viewing the transverse refractive index profile as shown in figure (3.15).

This trench works well for use of the fibre, when untapered, as the evanescent field of a mode is most predominant closest to the core and drops exponentially outwards. However if these fibres were to be tapered to micrometre diameters then undesired mode coupling can occur. This occurs when the original core becomes too small to trap modes but before the diameter of the cladding becomes small enough to become the new core with a new cladding of air. At this point the outer part of the cladding acts as another core due to it having a higher refractive index than the rest of the cladding. This results in loss as the fundamental mode of the original fibre cannot move adiabatically into the fundamental mode of the taper waist, as it couples into other modes during the taper transition. To combat this a pure silica core preform, with a uniformly flourine doped cladding, was fabricated by Draka using the plasma-enhanced chemical vapor deposition process. An optical fibre was drawn at the University of Bath using the fibre

fabrication tower that is described in section (2.2).

3.4.2 Germanium-free Fibre Fabrication Problems

Fibre that was drawn from the germanium-free preform did not perform as expected. The first fibre to be drawn, for my experiments, was to be a 1000 m in length with an outer diameter of 80 μm, as this was calculated to give a cut-off wavelength of 980 nm. This is so the solitons created from the 1064 nm pump are in the fundamental mode, which is needed in order to create the dispersive wave at the correct wavelength. It was requested by another party to draw another 1000 m of the fibre to an outer diameter of 125 μm. This was done first, before increasing the winder speed to reach an outer diameter of 80 μm. This point may seem mundane but it became vitally important for my research.

The fibre drawn to 80 μm outer diameter was of a very poor quality, both in its optical and physical properties. Physically it was fragile. Stripping polymer coating from an optical fibre is done using a razor blade and this is common practise. However, with this fibre it was extremely difficult to strip and not break the fibre inside. Cleaving a fibre can be done using a ceramic tile. The tile is used to etch the side of the fibre, once the polymer has been removed, which creates a defect that the fibre will break neatly at, resulting in a flat face. This flat face is important when coupling light in and out of an optical fibre. The germanium-free fibre that was successfully stripped of its coating

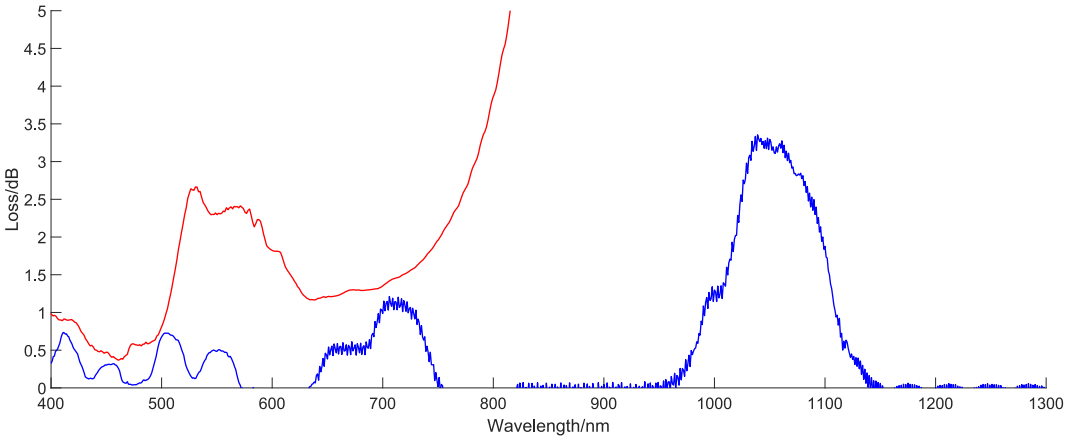

Figure 3.16 Bend loss measurements of two fibres fabricated from the germanium-free preform. Blue: loss measured from the first fibre drawn at 125 µm outer diameter. This fibre was bent into two circles of 3 cm diameter. Red: loss measured from a fibre drawn to 80 µm. This fibre was bent into one circle of 5 cm diameter.

would often snap when attempting to etch its side and did not give a flat face. When bending the optical fibre around a board marker, there was an audible cracking as the glass would snap many times but still be held together by the polymer coating. For reference a standard optical fibre can be wrapped tightly around a pencil and not break.

Optically the 80 µm fibre did not perform as expected. A white light source was coupled into it and the transmission was taken whilst the fibre was straight and when it had been bent into a circle that was 5 cm in diameter. The bent measurement was then taken away from the one taken whilst the fibre was straight and the results are shown as the red line in figure (3.16). Its loss past 800 nm is enormous. As a fibre that was designed to have a fundamental mode around 980 nm and transmit light up to 2 µm, this loss is unacceptable.

a) b)

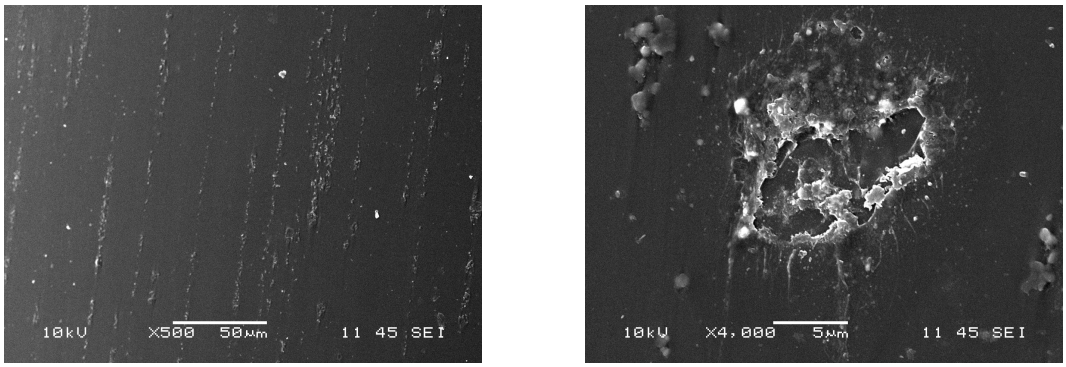

Figure 3.17 Scanning electron microscope images of a flourine clad cane that has been drawn from the preform down to a diameter of 2.5 mm. (a) taken at ×500 magnification and shows how the defects appear in parallel lines. These lines are longitudinally down the length of the cane. (b) taken at ×4000 magnification and shows one of the defects.

The blue line in figure (3.16) is a measurement taken using the first fibre drawn with an outer diameter of 125 µm. The fibre shows minimal loses with the exception of several peaks. Theses peaks indicate cut-off wavelengths for different modes. The largest peak, with its long wavelength edge at 1150 nm, is the loss from the second order mode and so corresponds to the fundamental cut-off wavelength. This is much more similar to what a bend loss measurement would look like for a standard optical fibre. This fibre also did not suffer from the physical weaknesses that the 80 µm outer diameter had despite being drawn under similar conditions.

The problems seen in the 80 µm outer diameter fibre could be viewed as an anomaly as the 125 µm fibre had none of the issues. However, further attempts at drawing fibre from the germanium-free preform had the same problems of

fragility and bad guidance. Variables such as the furnace temperature, feed rate, winder speed and tension in the drawn fibre were all investigated as possible causes but no solution was found. As part of this investigation some of the preform was drawn to a diameter of 2.5 mm and imaged under a scanning electron microscope. Two of these images are shown in figure (3.17). Figure (3.17) shows that there seem to be surface defects all along the glass. This could help to explain why the fibres were so fragile.

Another group working at the University of Bath later used a similarly flourine doped preform and were successful in drawing fibre that was both strong and guided as they desired (Harrington et al. 2017). It is their belief that the reason for this is that when they fabricated their fibre they drew very long lengths. This allowed the glass to reach an equilibrium of sorts. However, this doesn't explain why the 125 μm fibre discussed here works well whereas the 80 μm does not, as both were drawn for 1000 m.

Due to the lack of success in drawing a fibre with the desired cut-off wavelength of 980 nm, the 125 μm outer diameter fibre will be used for supercontinuum generation. Even though it has a different cut-off wavelength than SM980 it will still be able to show if light is generated below 380 nm

3.4.3 Germanium-free Fibre Results

Figure (3.18) shows the spectra produced by the pure silica core fibre. There are some clear differences that should be highlighted. The design of taper is

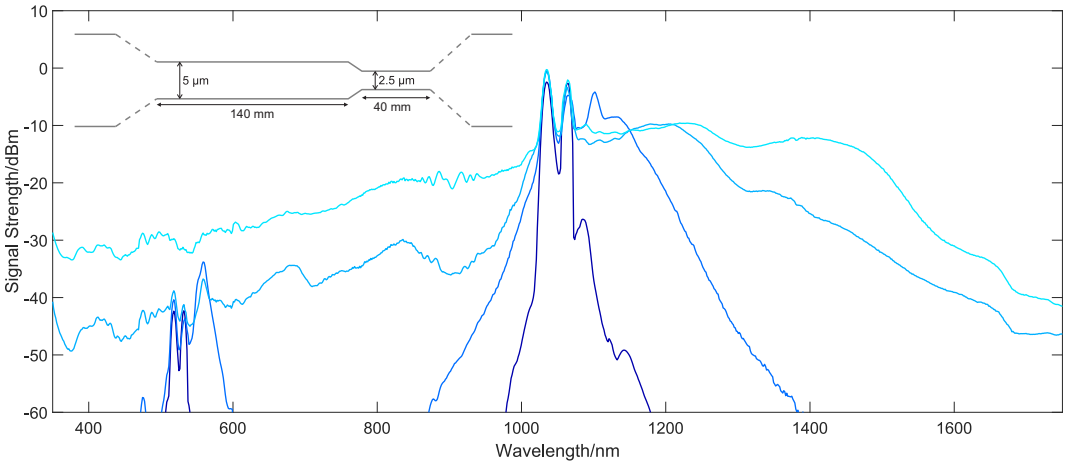

Figure 3.18 Spectra taken from a taper with two waist diameters of 5 and 2.5 µm. The waist with diameter of 5 µm has a length of 140 mm. The waist with diameter of 2.5 µm has a length of 40mm. The transition connecting the two different diameter waists has a length of 20 mm. Output powers are 10, 20, 50 and 70 mW, starting from the narrowest to broadest trace. The fibre used had no germanium dopant and instead a uniformly fluorine doped cladding.

the same as that for figure (3.13) but this spectra has spikes appearing several times below the pump wavelength and has a dip around 1380 nm. The reason for the spikes is unclear and may be the result of tapering a fibre with a different dopant profile than that for SM980 but this is only speculation. The dip in power around 1380 nm is because the cut-off frequency of the fibre is longer than the pump wavelength, at around 1150 nm. This was unintentional but, due to the difficulties described in (3.4.2), further fibre with a 980 nm cut-off could not be made.

The spectra shown in figure (3.18) does reach further into the short wavelengths. It is difficult to see exactly how far it extends but it is clearly further than tapers made with SM980 fibre.

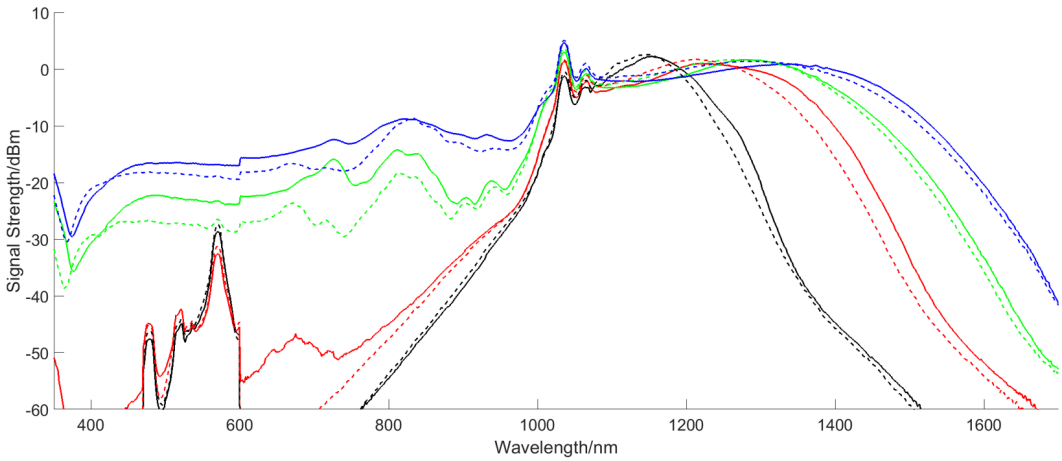

Figure 3.19 Spectra from two tapers with identical design but where a different flame has been used in the tapering process. The solid lines are for the taper made with an oxygen-butane flame and the dashed lines for an oxygen & deuterated-butane flame. Output power is shown by colour; black-20 mW, red-30 mW, green-50 mW, blue-70 mW.

3.5 Reducing the Waterpeak

A known problem when fabricating fibres is absorption caused by OH groups. This absorption is prominent at 1380 nm and is known as the waterpeak. This is also a problem when tapering fibres using a n-butane and oxygen flame as they burn to produce H_2O which can then enter the fibre. To see if reducing this loss affects the resulting supercontinuum the n-butane (C_4H_{10}) was replaced by deuterated butane (C_4D_{10}). This reduces the build up of OH groups and instead gives OD groups which have an absorption peak further into the infrared.

Figure (3.20) shows the absorption caused by a n-butane and oxygen flame in the blue line and is red is the result when the n butane has been replaced by

deuterated butane. It can be seen that the absorption has reduced the peak by 5 dB. Figure (3.19) shows the spectra from two tapers that have the same design but differ in what flame was used to taper them.

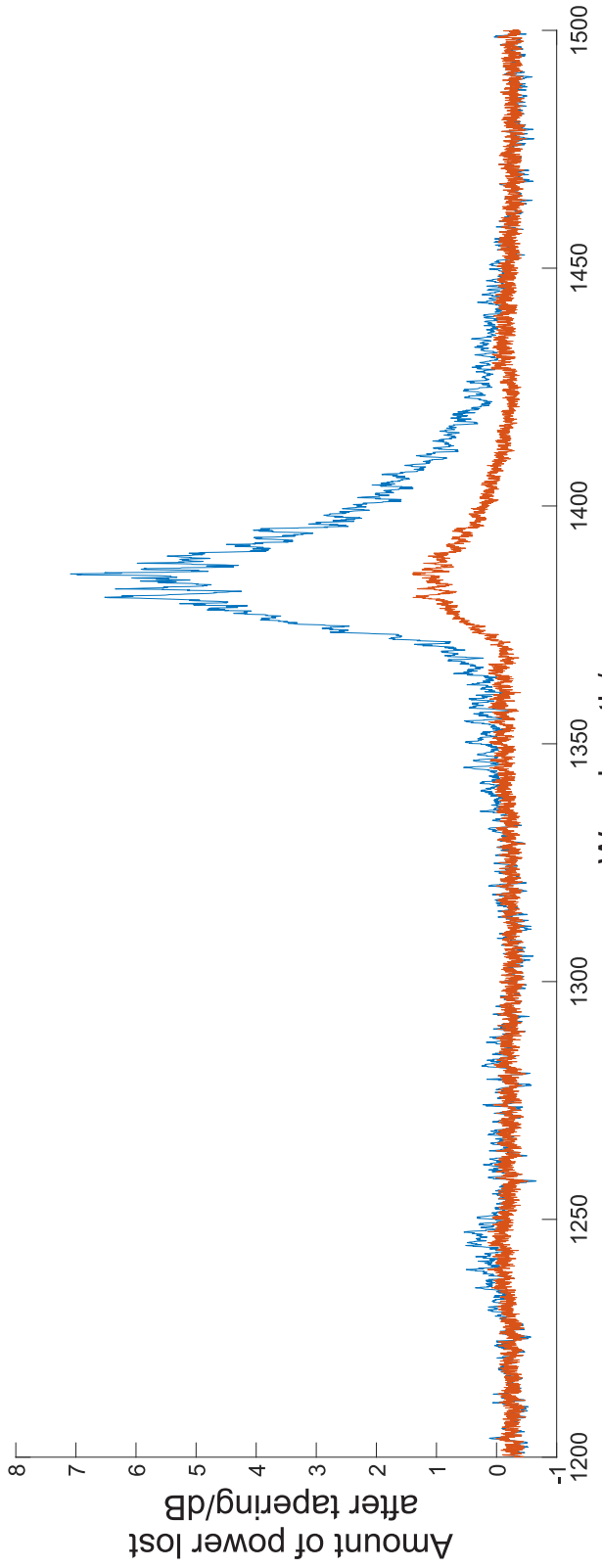

Figure 3.20 Absorption as a result of tapering SM980 down to a diameter of 5 µm over a length of 140 mm before transitioning down to a diameter of 2.5 µm for 40 mm. Blue line is the absorption when using a flame of n-butane and oxygen. Red line is the absorption when using deuterated butane and oxygen.

Chapter 4

Drilling Side Holes in Hollow-Core Fibres using an Oxygen-Butane Flame

4.1 Introduction

In this section hollow-core fibres were used to detect methane gas. The purpose behind this is to provide a system that can be used in underground mining operations to detect harmful gases, a common one being methane.

Optical fibres have been used for gas sensing for some time now. A problem with using a standard fibre is that very little electromagnetic field extends outside of the fibre to actually interact with any gases. Tapered fibres have been used as they have a much larger amount of their evanescent

field interacting with the air around the glass. Coating tapers with high index material can also enhance this effect (Wu et al. 2014).

Hollow-core fibres provide an opportunity as the core is not made of a solid glass but is hollow. This allows the core to be filled with a gas which has been done (Testa et al. 2018). In order to allow gases to enter the fibre along its length, holes can be drilled into the side using ultrafast lasers (Karp et al. 2016). To try and provide an alternative to using lasers, an oxygen-butane flame was used.

Once the side holes are made the fibre would be placed in an environment containing methane gas. By observing the transmission through the fibre it can be seen if the methane has successfully entered the fibre.

The hollow-core fibre was fabricated by Dr. R.J.A. Francis-Jones at the University of Bath. It was selected due to its transmission range, which includes 1600 - 1700 nm. It has an outer diameter of 125 μm and is of anti-resonant design, with 7 capillaries that surround the core.

4.2 Getting a Small Flame

The side holes would be made using the taper rig from section (3.1). However, The movable stages would not pull the fibre lengthwise and the burner would approach the fibre but not move along its length. The fibre was blocked at one end and nitrogen gas was inserted into the fibre at the other end in order to

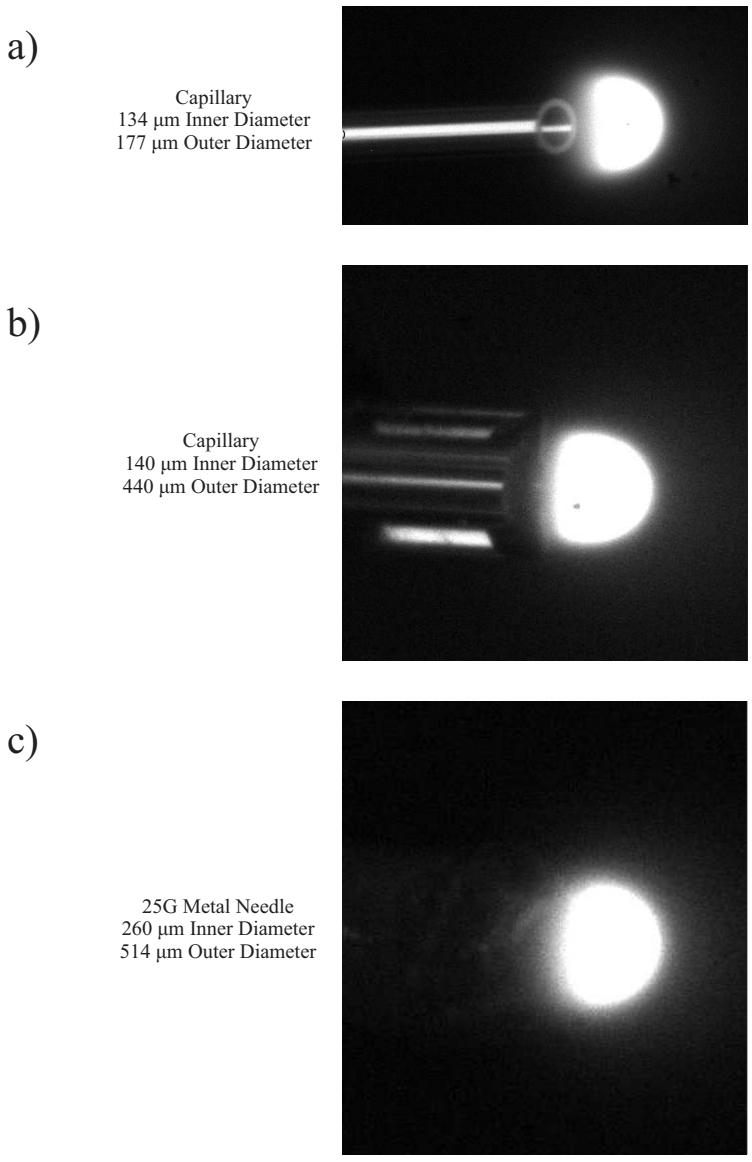

Figure 4.1 Photos taken of three flames from burners that were tested for use in burning side holes in hollow-core fibres. All photos are to the same scale. (a) and (b) are both made of glass capillaries with similar inner diameter but (b) has a outer diameter over twice as large. (c) a flame using a metal needle with an inner diameter of 260 µm.

pressurise the core. The reason for pressuring the core is that once the flame has heated a point on the fibre, until it softens, the pressure will push the side of the fibre out until it "pops" creates an opening. The attractive aspect of this method is the relative simplicity of its implementation. That is, if it works effectively then up-scaling its production would be a relatively simple task.

As optical fibres are thin, the side holes would have to be very small. In order to make a small hole, the flame used should be as small and pointed as possible. This is to minimise how much of the fibre is heated. Several burners were made from glass capillaries and metal hypodermic needles. Three examples of the smallest flames produced are shown to the same scale in figure (4.1). The size and shape of the flames are very similar, even in (4.1 c), where the inner diameter is almost twice the size of (a). The flames are ≈300 μm at their thickest and are not very pointy. The burner used to produce the flame in figure (4.1) (b) was chosen for the rest of the experiment as (c) was more difficult to light.

4.2.1 Method of Lighting the Burner

The process of creating the flames in figure (4.1) was not simple. Once the chosen burner was attached, the butane and oxygen flows were switched on. The amount of flow was unimportant so long as gas could be felt leaving the end of the burner. This was left unchanged for ≈1 minute to flush the gas pipes clean of atmospheric gas. The oxygen flow was then switched off.

A cigarette lighter was used for ignition of the burner. This was lit and brought in-line with the front of the burner but at a distance that would not ignite it. The lighter was slowly brought closer to the end of the burner but kept from touching. If the burner ignited then the lighter would be removed and a long yellow flame would be seen from the burner. If the burner did not ignite it would be because there was either too much or too little flow of butane. If there was too much butane flow, this would be evident from observing the flame of the lighter as it is pushed away from the burner. Otherwise there is too little butane flow and this would be increased before attempting to light again.

Once the burner is producing a long yellow flame, then came a balancing act. The oxygen flow needed to be increased to reduce the size of the flame (and to increase it's pointedness) but the total flow of the gases couldn't be too high else the flame would be too long or detach from the burner and extinguish. Care was taken during this process to avoid the flame burning up into the burner and so the flow of each gas was not adjusted simultaneously. If the flame did enter the burner then it could become damaged. The butane flow was first reduced to decrease the size of the yellow flame. Then oxygen flow was increased in small increments and after each change $\approx$10 seconds was allowed to pass to observe the flame and allow it to settle after each change. The target was to get a small pointy blue flame. If the flame was yellow then

it needed a greater ratio of oxygen to butane. If the flame was blue but too long, then the total amount of flow needed to be reduced.

It was found that each burner "preferred" a different ratio of oxygen to butane. Figure (4.1)(a) was taken at an oxygen to butane ratio of 4.8/1, (b) at 4.1/1 and (c) at 4.3/1. The total flow of gases was not calculated in this work.

4.3 Making the Side Holes

First it was attempted to make side holes in a capillary of glass. The capillary had an outer diameter of 1 mm and an inner diameter of 850 μm. Side holes were made with various amounts of pressure inside the capillary. Pressure was varied from 0.5 bar to 10 bar. It was found that higher pressures would result in a larger hole but sometimes less of the capillary would be distorted overall. Looking at figure (4.2) a bulge can be seen protruding from the side of the capillary. This begins to form when the flame is close enough to soften the glass. As the bulge begins to form, the flame would be retracted slowly to try and reduce the effect on the capillary but still keep the tip of the bulge soft.

The formation of the hole cannot be seen directly but it is obvious when it has happened as the expanding bulge immediately stops expanding and contracts slightly as the pressure has been released. The now escaping nitrogen gas can also be seen wafting, and sometimes extinguishing, the flame. The

higher the pressure, the quicker that this bulge would form. The retraction of the flame was done by hand and so keeping pace with a rapidly forming bulge, whilst also maintaining the correct precision, was difficult. At 10 bar the time from when the bulge begins to form until the hole has been created takes approximately 5 s whereas 0.5 bar could take up to 20 s.

To see if it would create less of a bulge the flame was retracted as soon as the capillary appeared to soften and then repeated until a hole was formed. It was found that although this method was easier to repeat, the bulge was consistently bigger.

A hole from a pressure of 0.5 bar is shown in figure (4.2 a) and is ≈75 μm in diameter. The bulge shown side-on in figure (4.2) (b) is quite symmetrical and approximately 0.7 mm in diameter. This was repeated several times along the length of the capillary and was easy to reproduce.

The same process was repeated on a capillary with an outer diameter of 500 μm and inner diameter of 425 μm. Several bulges with much the same shape as that in figure (4.2) were made. The holes were smaller, averaging around 50 μm and the bulges averaged 500 μm in diameter. This is still too big for the hollow-core fibre, which has a diameter of 125 μm, and would most likely significant impact the optical properties. Because the hole and bulge have reduced in size as the capillary has, it was deemed appropriate to at least attempt making side holes in the hollow-core fibre.

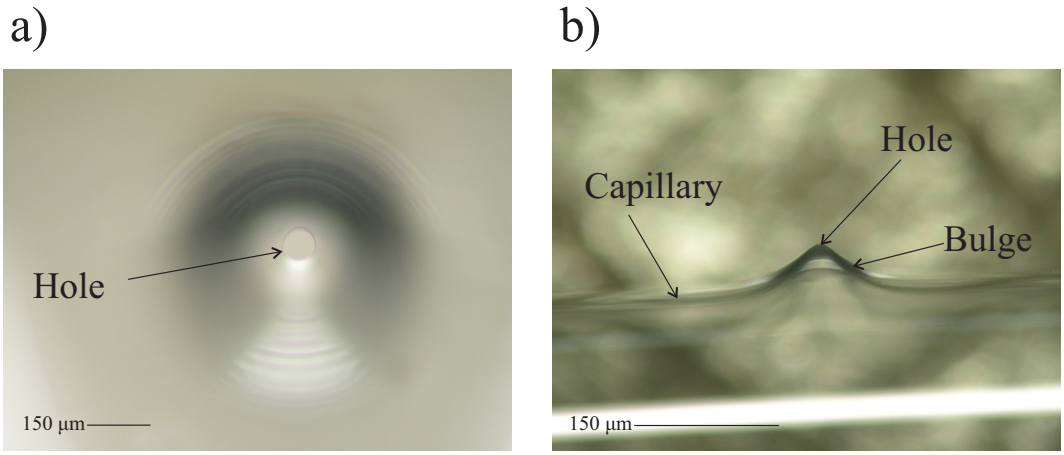

Figure 4.2 Photos taken through a microscope of a capillary with a hole made through pressurising the centre and applying a flame. (a) Top down view of the hole which measured ≈75 µm. (b) Side on view of the hole showing the bulge that was created.

Figure (4.3) shows the hole created in the side of a hollow-core fibre with a diameter of 125 µm. The hole is ≈60 µm in diameter however the symmetrical bulge seen when working with the capillaries is much different. Instead the entire cross-section of the fibre has been expanded and not uniformly. The part of the fibre closest to the flame has expanded the most.

It can be seen in figure (4.3 a) that the fibre to either side of the bulge has remained in line. This suggests that the fibre should still be able to transmit past the distortion due to the fibres long Rayleigh length. Looking closely at the resonators in figure (4.3 b), it can be seen that they expand away from one another and do not twist or merge together. In the cross sections nearest to the hole the resonators seemed to have disappeared altogether as they have most likely collapsed.

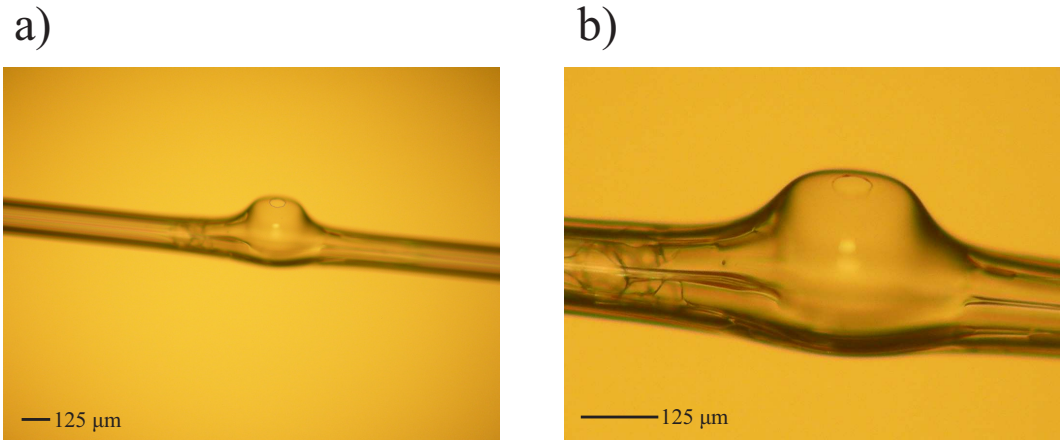

Figure 4.3 Photos taken through a microscope of a hollow-core fibre with a hole of ≈60µm made through pressurising the centre and applying a flame. (a) shows that the fibre remains straight either side of the distortion causes by creating the hole. (b) shows how the inside of the fibre, including the resonators, have been affected.

It was hoped that any defects caused by the creation of side holes would not cause a large amount of loss. As the hollow-core fibre has a very low NA, long Rayleigh length and if the fibre remains relatively straight, then a defect of the size seen in figure (4.3) will be similar to butt coupling the fibre on either side. The measured loss was 3 dB for this case although other holes, created in the same way, were found to have loss as high as 9 dB. This higher loss was attributed to the bulges moving the fibre on either side out of alignment of one another.

4.4 Detecting Methane

Four holes were made in a roughly 30 cm length of 1 m of hollow-core fibre and a xenon arc lamp (broadband white light source) was coupled into one

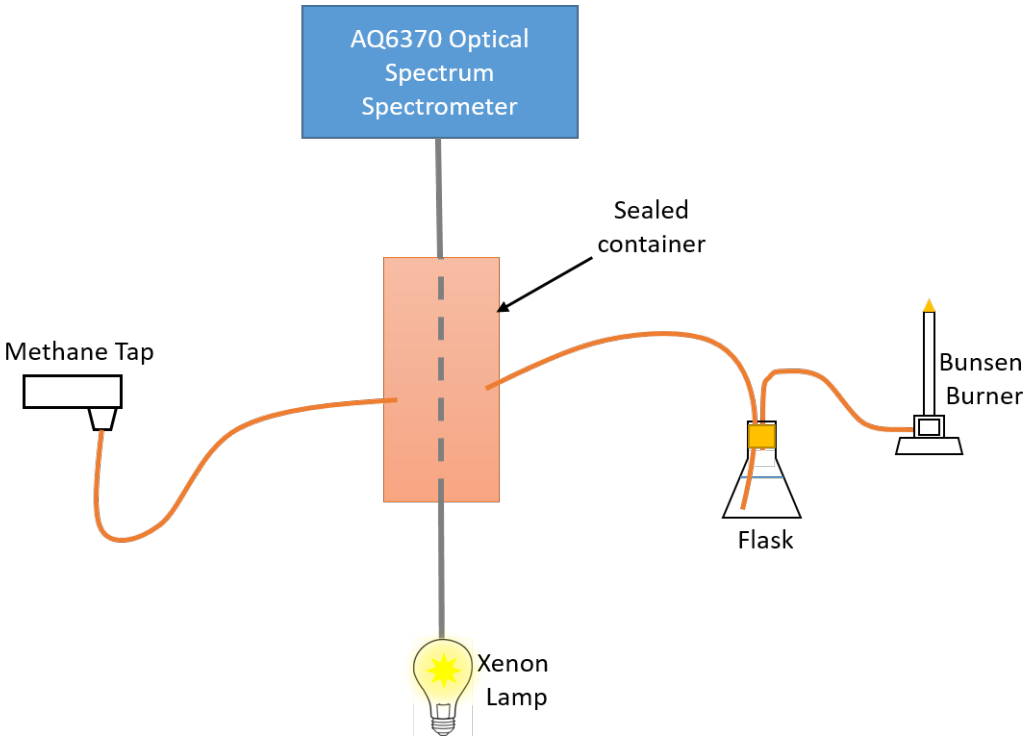

Figure 4.4 Schematic of experimental setup used to detect methane entering the hollow-core fibre through side holes.

end. The fibre was fed through a sealed container such that the fibre holes were situated within it. The other end was placed into a AQ6370 optical spectrum analyser set to a resolution of 0.5 nm. Using this low a resolution was undesirable as it would make identifying the absorption peaks more difficult but higher resolutions put the measured transmission too close to the noise floor of the optical spectrum analyser. A methane tap was connected to the sealed container to fill it with methane. To ensure that pressure did not build within the container, an overflow pipe was connected to a flask blocked with a cork. This overflow pipe was fed into the flask such

that it was submerged beneath the water that half filled the flask. Another pipe was fed through the cork but kept above the surface of the water and the other end was connected to a bunsen burner. By igniting the burner, any excess methane would exit the container and be burned off. A trace was taken on the optical spectrum analyser before and after the environment of the fibre was enriched with methane gas. Methane gas has several absorption peaks between 1600 - 1700 nm of varying strengths.

Figure (4.5) a) shows the results. The noise floor is just above -100 dBm. Several absorptions dips can be seen throughout the trace. The wavelength position of these dips match well with methane absorption data shown in figure (4.5) (b).

Figure (4.6) shows the transmission of the fibre after different lengths of time in the methane rich environment. It is apparent that the transmission was not stable, with several wavelengths from the 7-minute-measurement showing greater transmission than those of the 3 & 5 minute measurements. This was a problem throughout the experiment and is due to the amount of optical power being so close to the noise floor. To decrease this variation, the resolution of the spectrometer can be reduced (>0.5 nm) but the spectral width of absorption peaks are very narrow and it would be more difficult to detect them.

To investigate the reliability of the data recorded in this experiment four peaks were chosen at wavelengths of 1638, 1640, 1643 and 1645 nm. By

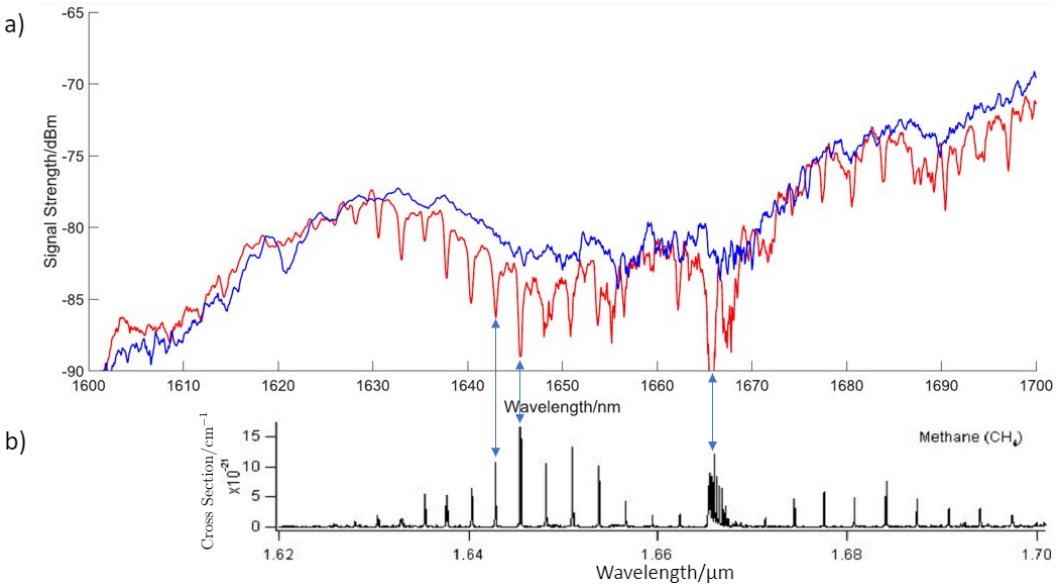

Figure 4.5 a) Transmission spectra of the hollow-core fibre at a resolution of 0.5 nm. Blue: Taken in the absence of methane. Red: Taken after the fibre has been in a methane rich environment for 11 minutes. b) Fourier-transform infrared spectroscopy of the cross-sections of methane taken from the PNNL database (2009). The two spectra have been aligned by their x-axis to show the matching of absorption to known data.

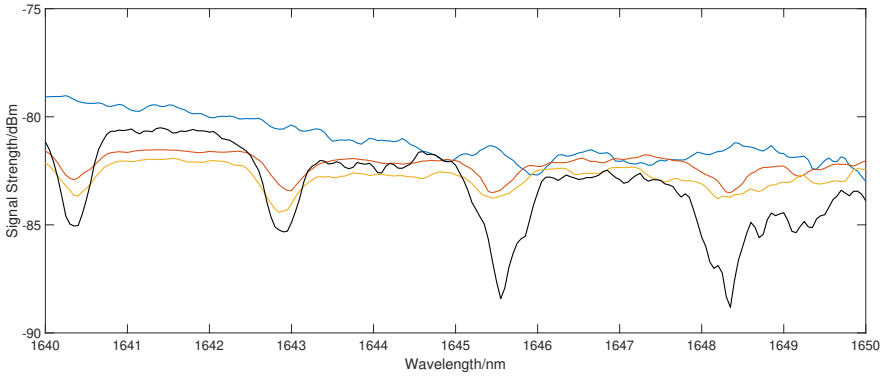

Figure 4.6 a) Transmission spectra of the hollow-core fibre at a resolution of 0.5 nm. Blue: Taken in the absence of methane. Red: Taken after the fibre has been in a methane rich environment for 3 minutes. Orange: Taken after the fibre has been in a methane rich environment for 5 minutes. Black: Taken after the fibre has been in a methane rich environment for 7 minutes.

calculating an effective path length of methane at 100 % concentration it is possible to make a judgement of the data, as the effective length at each of these peaks should be the same. The ratios of these peaks against background spectra were calculated in order to get the transmission and inverted to provide absorption as a percentage. This can be seen in table (4.1).

Wavelength/nm	Absorption/%	Effective Path Length/cm
1638	52	350
1640	62	90
1643	63	23
1645	59	15

Table 4.1 Approximate signal absorption at several wavelengths and effective path lengths as calculated using the application Bytran (Pliutau & Roslyakov 2017).

The HITRAN online database contains a vast amount of molecular absorption data including line-by-line spectroscopic parameters, infrared absorption cross-sections, collision-induced absorption data and more (Gordon et al. 2017). The application Bytran provides a user friendly interface to access the HITRAN database and allows the user to define meteorological conditions, instrument parameters, specify gas mixtures and the path length of signal in order to calculate absorption (Pliutau & Roslyakov 2017). Using this application it was possible to set the concentration of methane to 100%, temperature to 295 Kelvin, total pressure to 1 atm and spectrometer resolution to 0.5 nm. This was done in order to

match the databases absorption to the experimental results in figure (4.5)(a) by varying the path length. This allowed the estimation of the effective path length of methane within the fibre and the results are summarised in table (4.1). It was important to set parameters that were representative of the experiment as each affects the measured absorption:

- Temperature changes the amount of Doppler broadening in the absorption peaks (Chantry 1971).
- Spectrometer resolution affects the shape of the absorption peaks. Methane absorption peaks are far narrower than the 0.5 nm spectrometer resolution, which results in a flattening of the peaks.
- The total pressure was set to 1 atm which may not have been the case despite the presence of the overflow pipe but this is a reasonable .
- Finally, setting the concentration of methane to 100 % allows the calculation of an effective length of the fibre filled with pure methane.

The effective path lengths in table (4.1) have a wide range (>300 cm) and this is most likely due to the light levels being so close to the noise floor of the spectrometer. The absorptions in table (4.1) only vary by 10 % whereas the HITRAM database shows that the absorption at 1638 nm should be $1/8^{\text{th}}$ of that absorbed at 1643 nm.

4.5 Conclusions

It has been shown that an oxygen-butane flame can be used to form side holes in a hollow-core fibre by pressurising the core with nitrogen. The holes created in a 125 μm outer diameter anti-resonant hollow-core fibre were as small as 60 μm. However, in creation of the holes a significant amount of the fibre was distorted. Placing a hollow core fibre with four holes along its length, into a methane rich environment allowed the methane to be detected as it moved into the core of the fibre. The disruption of the guidance properties of the fibre meant that the amount of detected light was very close to the noise level of the spectrometer which severly hinders analysis of the results beyond the observation that there was absorption at wavelengths corresponding to the presence of methane.

Reducing the size of the burner that delivers the oxygen-butane mix can only reduce the size of the flame to a minimum of ≈300 μm. One way that this could perhaps be further reduced is by replacing the butane with hydrogen. Hydrogen burns faster than butane and so this should allow increased flow rates of the gases which may lead to a sharper flame.

The loss of 3 dB adds a difficulty to applying this method to a larger scale. Each hole added to the fibre further increases the loss and so must be compensated with a more powerful source, repeater systems or more sensitive detectors. If the desired area of detection is very large then the spacing of

holes along the fibre could be increased to help reduce the loss but this could mean a slower detection time.

Chapter 5

Maximising the Idler in Four-Wave Mixing

5.1 Introduction

In the following section I investigated four-wave mixing fibre with an interest in maximising the power in the idler. The four-wave mixing fibre used in this section was previously fabricated at the University of Bath (Wadsworth et al. 2004). It has a hole-to-hole pitch of Λ=0.3 μm and a hole diameter d such that $\frac{d}{\Lambda}$=0.3. A scanning electron microscope image of the cross section of the four-wave mixing fibre is shown in figure (5.2). The two larger holes above and below the core break the symmetry of the core such that it maintains the propagating light's polarisation. It was chosen as the phase matched idler wavelength for a 1064 nm pump should be just below 2 μm. Figure (5.1) is

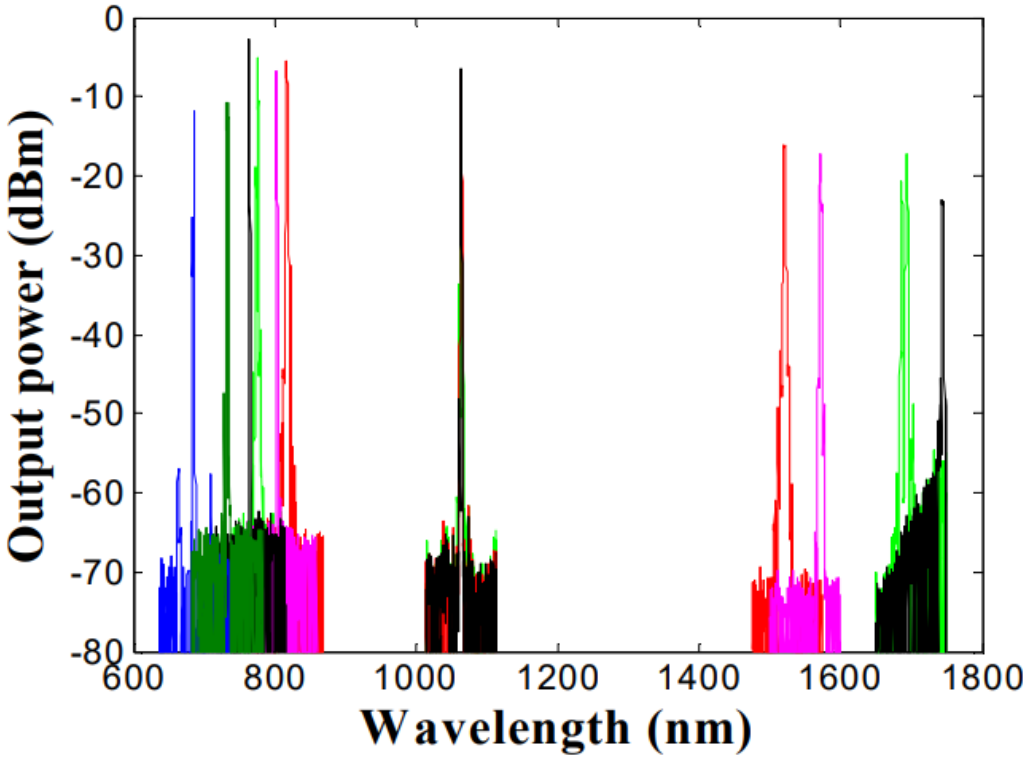

Figure 5.1 Output spectra for 3 m lengths PCFs A, C, F, G, H, I showing strong optical parametric generation in the normal dispersion regime, input power 10≈20 mW. Spectrometer resolution 0.2 nm. Idler wavelengths longer than 1750 nm are not measured with this spectrometer (Wadsworth et al. 2004).

taken from the Wadsworth et al. (2004) paper and shows the output spectra for the fibre used in this thesis (Fibre C in dark green) as well several others with varying hole diameter but equal pitch. Only the signal wavelength of the fibre is seen in this figure as the spectrometer used couldn't measure beyond 1750 nm but the earliest measurements of this investigation showed that the fibre produced an idler at a wavelength of ≈1910 nm, making it suitable for this investigation.

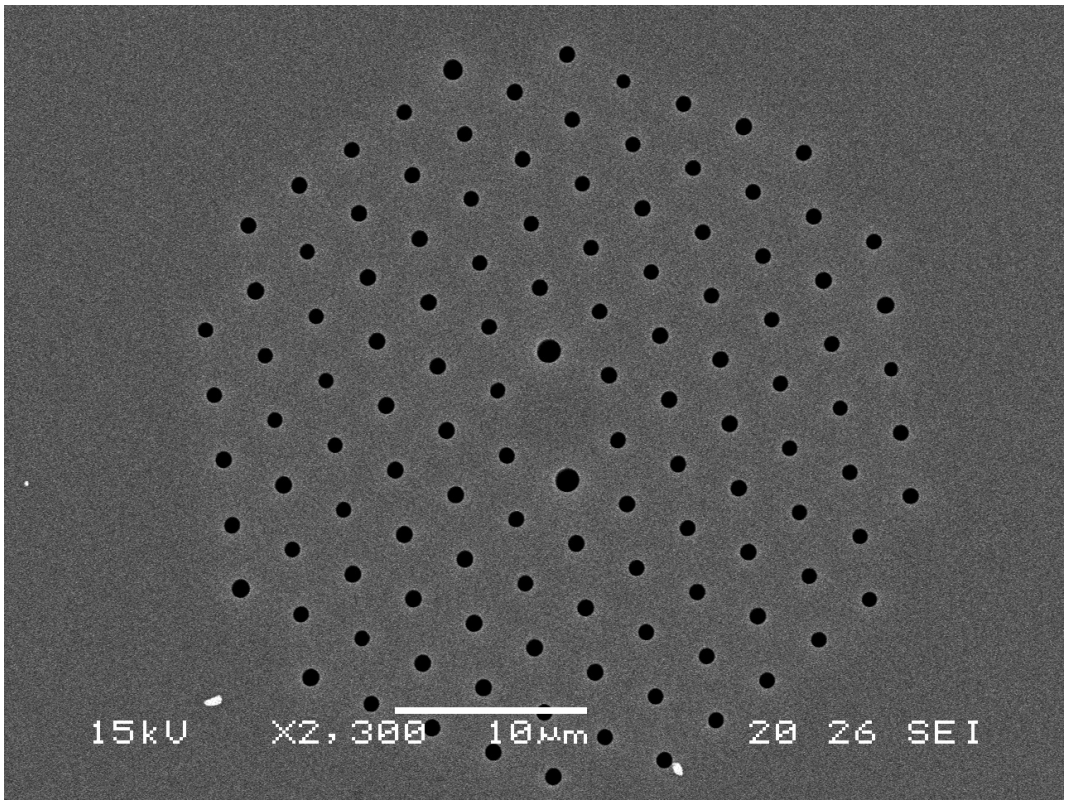

Figure 5.2 Scanning electron microscope image of the cross-section of the photonic crystal fibre used in generating this section.

5.2 Experimental Setup

The laser source used for this section was a 1064 nm Fianium master oscillator power amplifier system. It has an in built pulse picker allowing the variation of repetition rate. The maximum peak power of the pulses was around 2200 W. The fibre output was coupled into the four-wave mixing fibre through a splice. This splice had been optimised to maintain polarisation of the light by aligning the two fibres by their polarisation axes before splicing. Light exiting the four-wave mixing fibre was collected by an integration sphere and passed into

a Bentham DTMc300 double monochromator to measure the spectrum at a resolution of 5 nm. The spectrometer's spectral response was calibrated with a calibration halogen bulb.

Figure (5.3) shows the results from a length of 5 m of four-wave mixing fibre at different input powers at a repetition rate of 40 MHz. The signal and idler peaks can be seen in the 5.2 and 6.5 W input power traces at wavelengths of 735 nm and 1915 nm. The idler has a lower power than the signal. This is expected as the four-wave mixing process conserves photon number. This means that the number of photons at the signal wavelength should be the same as the number at the idler. A photon which is otherwise the same as another except in wavelength will have a different photon energy. Longer wavelength photons have less energy than shorter ones. Therefore the idler peak should always be lower than the signal unless there is uneven losses.

Other peaks can be seen that are the result of multi-mode and slow axis polarisation four-wave mixing such as at 895 or 1470 nm. These become more prominent at higher powers. The 6.5 W trace shows a supercontinuum ranging from ≈830 - 1500 nm. This occurs after the there has been sufficient Raman for solitons to form beyond the zero-dispersion wavelength. Soliton fission then occurs and a supercontinuum is generated in much the same way as in section (3).

There is a calibration error that was not quashed at 800 nm. There is a

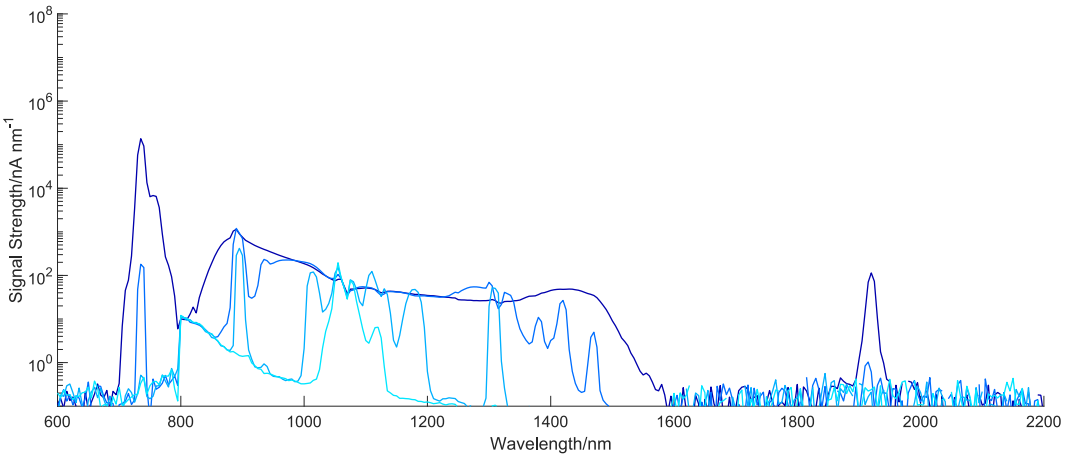

Figure 5.3 Output spectrum from 5m of four-wave mixing fibre. From lightest to darkest blue the input powers are 2.2, 3.5, 5.2 and 6.5 W. The repetition rate is 40 MHz.

discrete step as the monochromator changes detector. There is also a relatively substantial amount of power just above 800 nm that appears to be constant in the traces with a slight exception of the 6.5 W input power that rises above most of it. This could be light being picked up from the scattering of the pump which would explain why it doesn't vary much. Both of these problems are similar to those seen in section (3) spectra between 400 - 600 nm. Once again these errors are not in the areas of interest when analysing these spectra and so can be ignored.

To measure the power around the signal and idler wavelengths, of the four-wave mixing fibre, the setup in figure (5.4) was used. The coupling between the laser source and four-wave mixing fibre remains the same as that used to measure the spectrum. After passing through the four-wave mixing fibre and exiting into free space the light is collimated by a lens. This light is then

separated by wavelength using a set of three prisms. These were chosen and angled such that the 1950 nm idler would meet the angle of minimum deviation for all three.

The pump light is removed by a beam block before two thermal detectors measure power in the signal and idler. To confirm that the detectors are only measuring the idler and signal, they were moved across the area where the desired section of the spectrum was diffracted. This was done using the 6.5 W input power from figure (5.3) where it can be seen that the idler and signal peaks contain much more power than their surrounding wavelengths. So when moving the detector, the measured power should go from low to high to low. It is important that this happen over a small distance as to ensure that the detectors are collecting all of the power in the peaks.

The spectrum taken by the monochromator cannot be used to gather this data as it is not calibrated for power but the spectrum is calibrated to itself. This means that any spectra taken by this monochromator can be compared to others collected in the same way but cannot be compared to others. The fibre rotator used was a THORLABS HFR007 High Precision Bare Fiber Rotator and was used to rotate the output of the four-wave mixing fibre to minimise reflection from the prisms due to being close to the Brewster's angle.

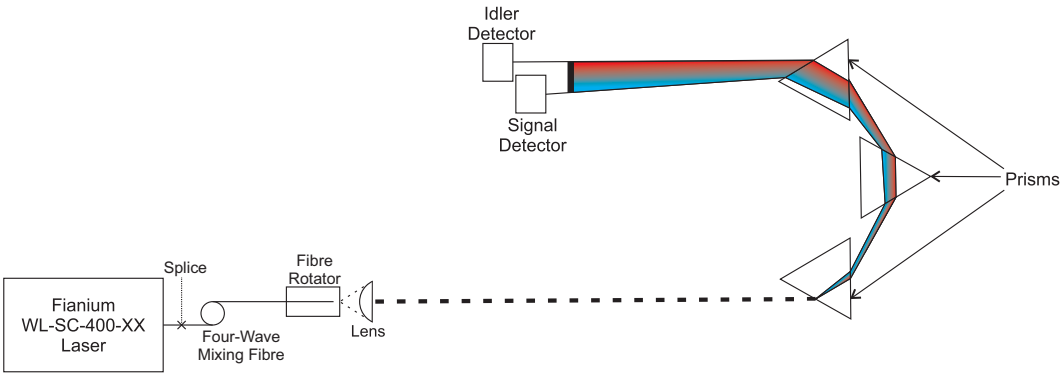

Figure 5.4 Diagram of experimental setup used to measure the power around the signal and idler wavelengths. The output from the four-wave mixing fibre is collimated by a lens and then seperated by three prisms. Pump light is blocked and the signal and idler wavelength powers are measured. In the diagram the seperation of wavelength is illustrated by a fade of red to blue. Blue indicating the shorter wavelength path and red the longer wavelengths.

5.3 Effect of length and repetition rate

5.3.1 Introduction

Measurements were taken for many lengths of fibre at three different repetition rates of 40, 20 and 10 MHz whilst changing the average power in order to keep the maximum peak power of the pulses at 2200 W. The purpose of this was to see the effect of changing length and repetition rate on power in the idler. Increasing the length should result in more nonlinearity. For a pulse to undergo a significant amount of nonlinear effects it must travel at least the nonlinear length given by equation (2.20). If the peak power and nonlinear parameter remains the same then to increase the amount of nonlinearity experienced by a pulse the fibre length must be increased. Changing the repetition rate should

have no effect on the amount of nonlinear processes (if the peak power of the pulses is kept identical) but this investigation was done to see if there were any second-order effect from the equipment.

5.3.2 Results

Figure (5.5) shows the results for different lengths of four-wave mixing fibre at the same input power and repetition rate. The length of fibre with the highest power in the idler is 2 m. It was stated earlier that an increase in length increases the amount of non linear processes including four-wave mixing but 5 m gave less power in the idler than 2 m. This could be explained by the appearance of other four-wave mixing peaks that appear at longer lengths that could be taking power from the idler or could be the result of confinement loss which will be explained in section (5.4.2). The power in the signal continues to rise and doesn't drop at longer lengths. This shows that power at the idler is still being produced due to four-wave mixing being a process that conserves photon number.

Figure (5.6) shows results taken from 2 m of the four-wave mixing fibre at different repetition rates. They are very similar and overlap one another over the majority of the wavelength range. Decreasing the repetition rate increases the energy in each pulse but should not affect the pulse duration. This would lead to an increase in peak power which would cause more nonlinearity. Too high a peak power however, would result in damage to the laser system. So

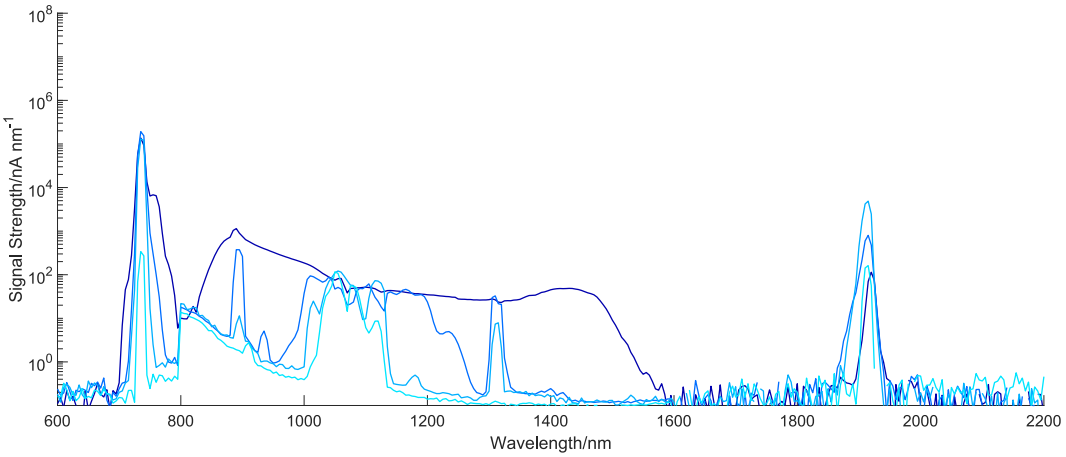

Figure 5.5 Output spectrum from several lengths of four-wave mixing fibre all taken with an input power of 6.5 W and at a repetition rate of 40 MHz. From lightest to darkest blue the lengths are 5, 3, 2 and 1 m.

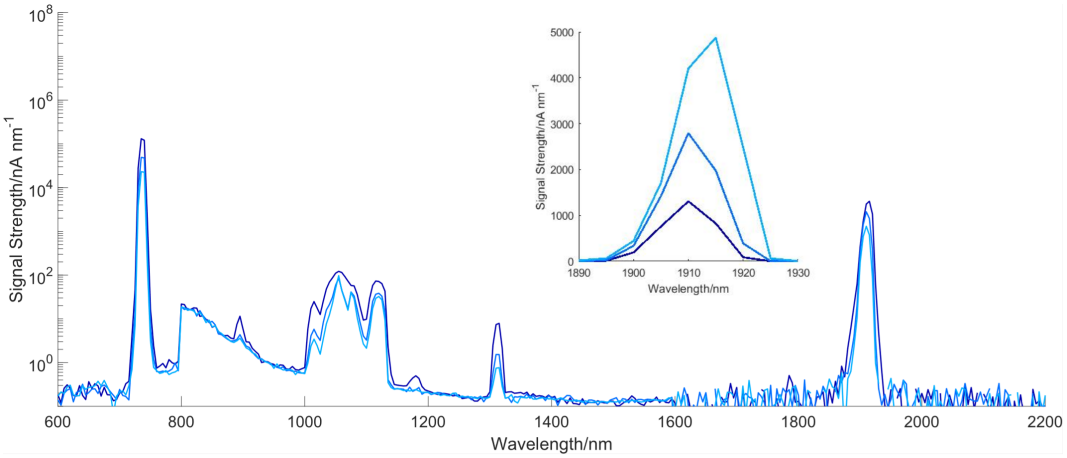

Figure 5.6 Output spectrum from 2 m of four-wave mixing fibre at various repetition rates. From lightest to darkest blue the repetition rates are 10, 20 and 40 MHz. Input power is set to 1.5 W for 10 MHz, 3.2 W for 20 MHz and 6.5 W for 40 MHz. These powers result in pulses of energy 0.15 µJ, 0.15 µJ and 0.16 µJ respectively. Inset into this figure is a zoom of the idler peaks with the y-axis having a linear scale.

when lowering the repetition rate, the maximum average power is lowered as well. This was done such that for each of the repetition rates shown in figure (5.6), the pulses should be almost identical which is evident in that the spectra are so similar.

Looking at the inset to figure (5.6), its the 40 MHz result that has the highest power followed by 20 and then 10 MHz. This is not significant as this is the case over the entire range of the measurement. This suggests that it is due to the differences in average power.

As the pulses were being kept so similar it was expected that the difference in the resultant spectra would be minimal and this is shown in figure (5.6). This investigation was done however to see if there were any other affects in changing the repetition rate. For example, the average power was higher when the laser was operating at 40 MHz and so there would be greater heat generated. This could have manifested in a slight changed in the pumps wavelength or greater loss in the splice connecting the four-wave mixing fibre, neither of which was observed.

Lower repetition rate also means more time between pulses. If this time reached a value that was similar to the relaxation time of the energy states within the fibre amplifier then there would have been a significant increase in the amount of amplified spontaneous emission.

5.4 Effect of Pulse duration

5.4.1 Introduction

In this section the pulse duration of the laser system was altered by changing the amount of power going to the oscillator. Although unable to measure the pulse duration the range as specified for the system was 37 - 90 ps. Using an autocorrelator I was able to confirm that 37 ps was the duration of the shortest pulse. The autocorrelator could not measure any pulses longer than 45 ps as it was not designed to. All data was collected at a repetition rate of 40MHz. By changing the pulse duration of the system but keeping average power the same, peak power of the pulses is affected. The maximum output power from the laser for the two shortest pulses was reduced in order to not cause damage to the laser system.

5.4.2 Results

Looking at figure (5.7) it can be seen that shorter pulse duration causes the signal to reach higher powers for the same input power. This makes sense as the peak power of these pulses is higher. However figure (5.8) does not show the same relationship for the idler power. Shorter pulses do initially give more idler power at low input power but with the exception of the three longest pulses they all form a plateau at the higher powers. This could suggest that the four-wave has been exhausted but figure (5.7) shows that this is not the

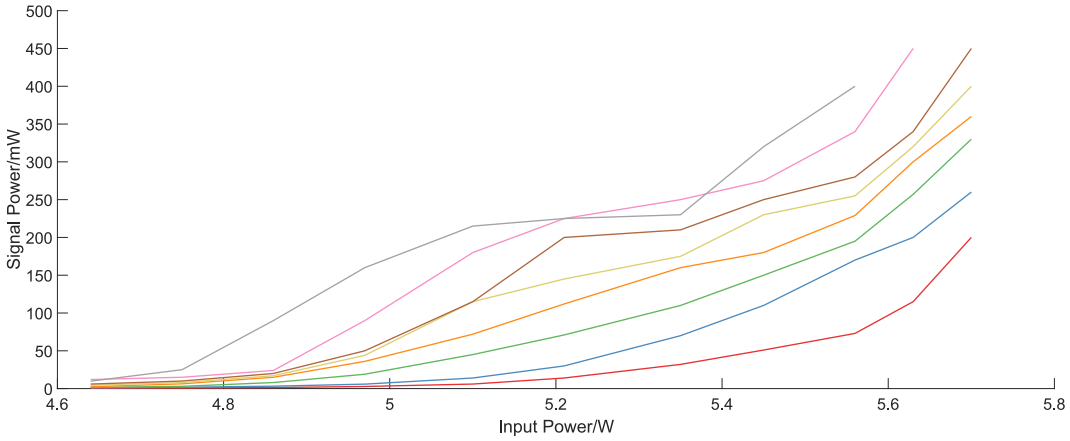

Figure 5.7 Power of signal against input power for 2 m of fibre with pulse durations ranging from 37 - 90 ps. From longest to shortest pulse duration: Red, Blue, Green, Orange, Yellow, Brown, Pink, Grey.

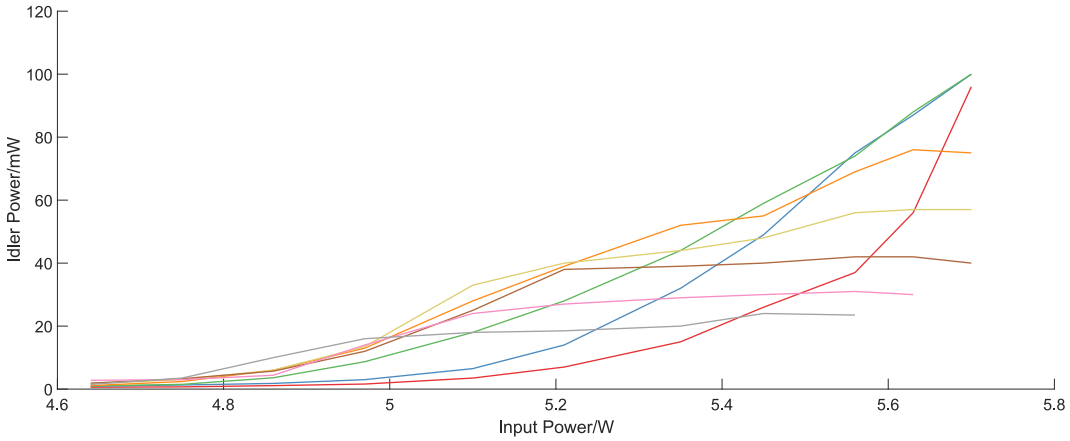

Figure 5.8 Power of idler against input power for 2 m of fibre with pulse durations ranging from 37 - 90 ps. From longest to shortest pulse duration: Red, Blue, Green, Orange, Yellow, Brown, Pink, Grey.

case and so photons must still be generated at 1915 nm in order to satisfy the conservation of photon number.

One of the four-wave mixing peaks shown in figure (5.5) (that is, not the ones at 735 or 1915 nm) could be the result of phase matching involving the 1915 nm idler. This could explain the plateaus as photons would still be produced at 1915 nm but also taken away by another four-wave mixing process and so satisfying the conservation of photon number.

It could be that the photonic crystal fibre has a high confinement loss at the idler wavelength and so although photons are produced they then escape the fibre. This theory suggests that for pulse durations that do not plateau then a large amount of four-wave mixing is occurring in a small length at the end of the fibre. This would be while the rate of generation is larger than the rate of loss. Figure (5.9) and (5.10) show power from the signal and idler after 20 cm has been removed. The exact powers may vary a lot when compared to figure (5.8) which could be unrelated to the amount of four-wave mixing for example an imperfect cleave or greater loss from the prisms if the fibre is not rotated as well will cause this difference. The power of each point is not the important measure here as we are looking for when the plateaus form. The pulse duration shown in orange doesn't seem to reach a plateau and is still climbing whereas in (5.8) its seems to be slowing down from the input power of 5.56 W upwards.

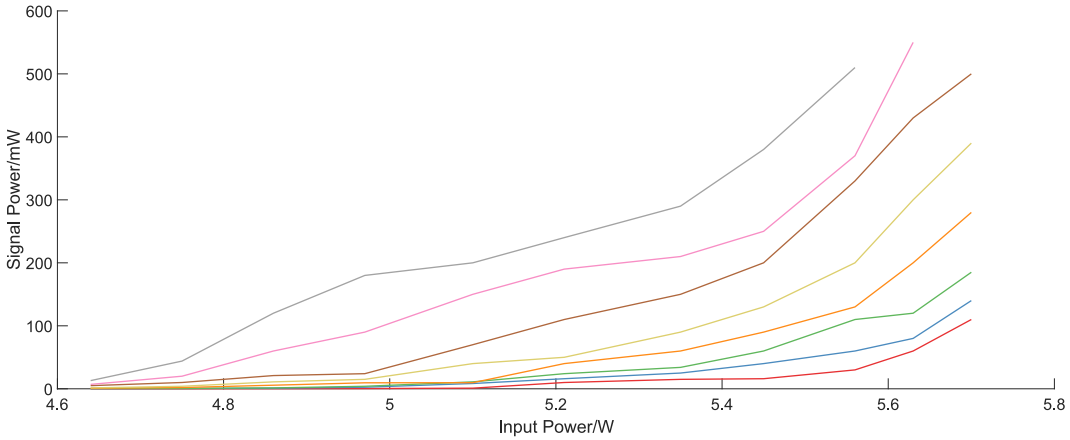

Figure 5.9 Power of signal against input power for ≈1.8 m of fibre with pulse durations ranging from 37 - 90 ps. From longest to shortest pulse duration: Red, Blue, Green, Orange, Yellow, Brown, Pink, Grey.

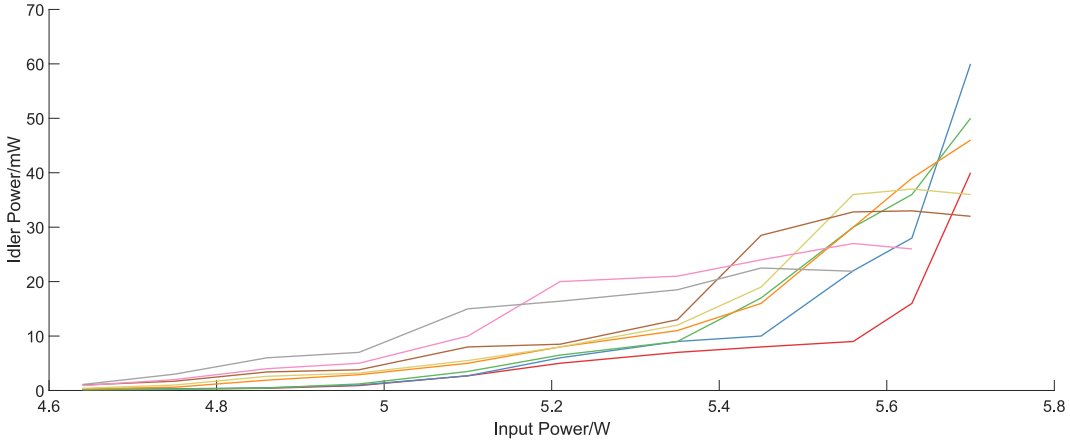

Figure 5.10 Power of idler against input power for ≈1.8 m of fibre with pulse durations ranging from 37 - 90 ps. From longest to shortest pulse duration: Red, Blue, Green, Orange, Yellow, Brown, Pink, Grey.

5.5 Conclusions

A 1064 nm master oscillator power amplifier laser system that delivered pulses with durations of the order of a few tens of picoseconds and with peak powers around 2200 W were used in a four-wave mixing fibre to generate over 100 mW of power at the idler of 1915 nm. The relative simplicity of the master oscillator power amplifier over laser systems of other designs is appealing.

Generating idler power in the near infrared, using a photonic crystal fibre has several factors that can be changed in order to optimise. If you want to have more average power then a higher repetition rate can be used. Having lots of peak power and long lengths of fibre may seem desirable, as there will be more nonlinearity and so more four-wave mixing, but there is a point where power is lost from the idler. This means that the length of fibre used should be matched to the peak power of the system.

The theory of confinement loss may be true but further investigation is needed. Perhaps a look at the best lengths for each pulse duration and then a comparison of how much idler power is generated would help. If there is confinement loss then shorter pulses with shorter lengths of fibre should be better than longer pulses with longer fibre. This would be due to more length giving more loss.

Chapter 6

Conclusions and Future Work

In this thesis I have investigated the processes involved in soliton based supercontinuum generation, the applicability of oxygen-butane flames in creating side holes for hollow-core optical fibre and the maximisation of power in the idler wavelength of four-wave mixing within a photonic crystal fibre.

The work in chapter (3) shows the usefulness of tapered optical fibre in a study of soliton based supercontinuum generation. Tapers were made with taper waists up to 250 mm in length at diameters as low as 1 μm. Previous supercontinuum generating tapers produced by the University of Bath were limited to ≈90 mm taper waist lengths due to the limits of the in-house taper rig(Birks et al. 2000). Since then the taper rig has been altered to allow longer waist lengths which this thesis has shown can be done down to the diameters necessary to allow soliton based supercontinuum generation from a 1064 nm

pump source. Spectra collected in this thesis are all directly comparable with one another as the output and input coupling is identical. This is an advantage over data collected from photonic crystal fibres where the output and input coupling is different for each fibre.

Work focused on the generation of short wavelengths, resulted in a non-uniform taper waist that decreased in diameter in the direction of propagation to maximise the amount of light towards the UV end of the spectrum. The low wavelength edge of the supercontinuum reached close to an absorption peak of germanium at ≈380nm and so a germanium-free fibre was fabricated and tapered to see if light could be generated at even lower wavelengths which they did.

Loss due to waterpeak absorption was investigated as the tapering process used an oxygen-butane flame which increased absorption at 1380 nm. It was found that the increased absorption did not significantly affect the overall loss of the tapers and had little to no effect on the shape of the generated supercontinua.

The process used in this thesis to make tapers was quick and it kept standard fibre on either end of the taper which eased coupling. These factors could be intriguing for industrial applications. It is not implausible to imagine mass customisation of supercontinuum sources, with customers having the option to request custom spectra. Of course there are limits to

what can be done but taking the examples shown in thesis, if a customer wanted a supercontinuum between 700 - 1300 nm at lower powers then figure (3.9) (c) shows a 5 μm uniform taper that would satisfy this. Photonic crystal fibres could also be ordered to satisfy these requirements but the coupling would be different between different photonic crystal fibres whereas no matter the taper shape, the coupling would always be the same which would significantly aid industrial integration.

The main drawback of tapers is their fragility and further investigation into increasing lifespan would have to be undertaken. This investigation could look at making the tapers within a clean room and sealing the vulnerable taper waists within hermetically sealed 'black boxes' with standard fibre input and outputs.

Chapter (4) showed that it was possible to use a premixed oxygen-butane flame to create side holes in a pressurised 125 μm outer diameter hollow-core optical fibre such that methane gas could diffuse into the core. Using hollow core optical fibres for use in gas sensing is a current area of interest in the scientific community where the most common method of creating side holes (to allow the gases to enter the core) involves laser drilling (Yang et al. 2017, Hodgkinson & Tatam 2013). Although side holes have been created in the side of hollow core fibre using laser drilling, no work has been previously done in using a flame as the heat source. The side holes disturbed the optical properties

of the fibre and were the source of significant loss. The same method allowed creation of side holes in capillaries of larger size, with the smallest capillary having a 500 μm outer diameter. Holes as small as ≈50 μm were made with minimal deformation of the capillary.

Further work into this could be the use of fuel with a faster burn rate. This should allow the premixed gases to still burn whilst at a higher flow rate which could give a shaper flame. This may allow the creation of side holes that damage the hollow-core fibre less.

Replacing the hollow core fibre with one that has an outer diameter more similar to the capillaries tested in this thesis (≈500 μm) may allow the creation of side holes that does not affect the guidance properties so severely.

It would be interesting to investigate the influence of thickness that the outer layer of the fibres has on side hole creation. Using capillaries fabricated to have the same outer diameter but varying inner diameter would avoid the complication of fabricating hollow-core fibre.

Chapter (5) gives experimental evidence to how four-wave mixing is affected by pulse repetition rate and suggests an importance of matching the pulse width to the length of four-wave mixing fibre. The investigation used a 1064 nm master oscillator power amplifier laser system that delivered pulses with ≈2200 W peak power to generate over 100 mW of idler power at 1915 nm. This kind of investigation has not been publicised to the knowledge

of this theis' author. The experimental setup used could be seen as a precursor a spliced all fibre mid-infrared seed source, which could be useful as an alternative to thulium sources (Russell et al. 2018, Hoult 2015).

During this investigation evidence was found for confinement loss of the idler. This took the form of longer lengths of four wave mixing fibre resulting in less idler power, suggesting that the idler is escaping and being lost. Further investigation into this could be done by finding what length of fibre gives the highest idler power for several peak powers. It would be interesting to see what relationship peak power and length have in the setup used within this thesis, seeing as the basic theory suggests that the longer the length of fibre the more power will be transferred to the idler. If confinement loss is the culprit then to get the maximal amount of power in the idler then a pulse with a high peak power in a shorter length of fibre will be better than a low peak power pulse in a long length of fibre.

References

Abramov, I. S., Gospodchikov, E. D. & Shalashov, A. G. (2018), 'Extreme-Ultraviolet Light Source for Lithography Based on an Expanding Jet of Dense Xenon Plasma Supported by Microwaves', *Physical Review Applied* **10**(3).

Agrawal, G. P. (1990), 'Effect of intrapulse stimulated raman-scattering on soliton-effect pulse-compression in optical fibers', *Optics Letters* **15**(4), 224–226.

Agrawal, G. P. (2000), *Nonlinear Fiber Optics*, Vol. 542.

Akhemediev, N. & Karlsson, M. (1995), 'Cherenkov radiation emitted by solitions in optical fibers', *Physical Review A* **51**(3), 2602–2607.

Awang, N. A., Ahmad, H., Latif, A. A., Zulkifli, M. Z., Ghani, Z. A. & Harun, S. W. (2010), 'O-band to C-band wavelength converter by using four-wave mixing effect in 1310 nm SOA', *Journal of Modern Optics* **57**(21), 2147–2153.

Bariain, C., Matias, I., Arregui, F. & Lopez-Amo, M. (2000), 'Tapered optical-fiber-based pressure sensor', *Optical Engineering* **39**(8), 2241–2247.

Belli, F., Abdolvand, A., Chang, W., Travers, J. C. & Russell, P. S. J. (2015), 'Vacuum-ultraviolet to infrared supercontinuum in hydrogen-filled photonic crystal fiber', *OPTICA* **2**(4), 292–300.

Birks, T. A. & Li, Y. W. (1992), 'The shape of fiber tapers', *Journal of Lightwave Technology* **10**(4), 432–438.

Birks, T. A., Wadsworth, W. J. & Russell, P. S. (2000), 'Supercontinuum generation in tapered fibers', *Optics Letters* **25**(19), 1415–1417.

Burns, W., Abebe, M. & Villarruel, C. (1985), 'Parabolic Model for Shape of Fiber Taper', *Applied Optics* **24**(17), 2753–2755.

Carlson, D. R., Hickstein, D. D., Lind, A., Olson, J. B., Fox, R. W., Ludlow, A., Li, Q., Westly, D., Leopardi, H., Fortier, T., Srinivasan, K., Diddams, S. & Papp, S. B. (2017), Dispersion-Engineered Silicon Nitride Supercontinuum for Frequency Comb Metrology at the 10(-15) Level, *in* '2017 Conference

on Lasers and Electro-Optics (CLEO)', Conference on Lasers and Electro-Optics, IEEE. Conference on Lasers and Electro-Optics (CLEO), San Jose, CA, MAY 14-19, 2017.

Chantry, P. (1971), 'Doppler Broadening in Beam Experiments', *Journal of Chemical Physics* **55**(6), 2746–&.

Chen, J. & Gao, S. (2015), 'Wavelength-assignable 1310/1550 nm wavelength conversion using completely phase-matched two-pump four-wave mixing in a silicon waveguide', *Optics Communications* **356**, 389–394.

Chu, Z., Liu, J., Wang, K. & Yao, J. (2010), 'Four-wave mixing model solutions for polarization control of terahertz pulse generated by a two-color laser field in air', *Chinese Optics Letters* **8**(7), 697–700.

Coen, S., Chau, A. H. L., Leonhardt, R., Harvey, J. D., Knight, J. C., Wadsworth, W. J. & Russell, P. S. J. (2002), 'Supercontinuum generation by stimulated Raman scattering and parametric four-wave mixing in photonic crystal fibers', *Journal of the Optical Society of America B-Optical Physics* **19**(4), 753–764.

Datta, P., Matias, I., Aramburu, C., Bakas, A., Lopez-Amo, M. & Oton, J. (1996), 'Tapered optical-fiber temperature sensor', *Microwave and Optical Technology Letters* **11**(2), 93–95.

Dimmick, T., Kakarantzas, G., Birks, T. & Russell, P. (1999), 'Carbon dioxide laser fabrication of fused-fiber couplers and tapers', *Applied Optics* **38**(33), 6845–6848.

Ding, L., Belacel, C., Ducci, S., Leo, G. & Favero, I. (2010), 'Ultralow loss single-mode silica tapers manufactured by a microheater', *Applied Optics* **49**(13), 2441–2445.

Dudley, J. M., Genty, G. & Coen, S. (2006), 'Supercontinuum generation in photonic crystal fiber', *Reviews of Modern Physics* **78**(4), 1135–1184.

Dumais, P., Gonthier, F., Lacroix, S., Bures, J., Villeneuve, A., Wigley, P. G. J. & Stegeman, G. I. (1993), 'Enhanced self-phase modulation in tapered fibers', *Optics Letters* **18**(23), 1996–1998.

Ere-Tassou, M., Przygodzki, C., Fertein, E. & Delbarre, H. (2003), 'Femtosecond laser source for real-time atmospheric gas sensing in the UV-visible', *Optics Communications* **220**(4-6), 215–221.

Ermolov, A., Mak, K. F., Frosz, M. H., Travers, J. C. & Russell, P. S. J. (2015), 'Supercontinuum generation in the vacuum ultraviolet through dispersive-wave and soliton-plasma interaction in a noble-gas-filled hollow-core photonic crystal fiber', *Physical Review A* **92**(3).

Foster, M. A., Dudley, J. M., Kibler, B., Cao, Q., Lee, D., Trebino, R. & Gaeta, A. L. (2005), 'Nonlinear pulse propagation and supercontinuum generation in photonic nanowires: experiment and simulation', *Applied Physics B-Lasers and Optics* **81**(2-3), 363–367.

Foster, M. A., Moll, K. D. & Gaeta, A. L. (2004), 'Optimal waveguide dimensions for nonlinear interactions', *Optics Express* **12**(13), 2880–2887.

Foster, M. A., Turner, A. C., Lipson, M. & Gaeta, A. L. (2008), 'Nonlinear optics in photonic nanowires', *Optics Express* **16**(2), 1300–1320.

Frosz, M., Bang, O., Bjarklev, A., Andersen, P. & Broeng, J. (2005), Supercontinuum generation in photonic crystal fibers: The role of the second zero dispersion wavelength, *in* '2005 Conference on Lasers & Electro-Optics (CLEO), Vols 1-3', pp. 1255–1257. Conference on Lasers and Electro-Optics (CLEO), Baltimore, MD, MAY 22-27, 2005.

Gao, S., Wang, Y., Sun, R., Li, H., Tian, C., Jin, D. & Wang, P. (2014), 'Ultraviolet-enhanced supercontinuum generation in uniform photonic crystal fiber pumped by a giant-chirped fiber laser', *Optics Express* **22**(20), 24697–24705.

Gorbach, A. V. & Skryabin, D. V. (2007), 'Theory of radiation trapping by the accelerating solitons in optical fibers', *Physical Review A* **76**(5).

Gordon, I. E., Rothman, L. S., Hill, C., Kochanov, R. V., Tan, Y., Bernath, P. F., Birk, M., Boudon, V., Campargue, A., Chance, K. V., Drouin, B. J., Flaud, J. M., Gamache, R. R., Hodges, J. T., Jacquemart, D., Perevalov, V. I., Perrin, A., Shine, K. P., Smith, M. A. H., Tennyson, J., Toon, G. C., Tran, H., Tyuterev, V. G., Barbe, A., Csaszar, A. G., Devi, V. M., Furtenbacher, T., Harrison, J. J., Hartmann, J. M., Jolly, A., Johnson, T. J., Karman, T., Kleiner, I., Kyuberis, A. A., Loos, J., Lyulin, O. M., Massie, S. T., Mikhailenko, S. N., Moazzen-Ahmadi, N., Mueller, H. S. P., Naumenko, O. V., Nikitin, A. V., Polyansky, O. L., Rey, M., Rotger, M., Sharpe, S. W., Sung, K., Starikova, E., Tashkun, S. A., Vander Auwera, J., Wagner, G., Wilzewski, J., Wcislo, P., Yu, S. & Zak, E. J. (2017), 'The HITRAN2016 molecular spectroscopic database', *Journal of Quantitative Spectroscopy & Radiative Transfer* **203**(SI), 3–69.

Gordon, J. P. (1986), 'Theory of the soliton self-frequency shift', *Optics Letters* **11**(10), 662–664.

Harrington, K., Yerolatsitis, S., Van Ras, D., Haynes, D. M. & Birks, T. A. (2017), 'Endlessly adiabatic fiber with a logarithmic refractive index distribution', *OPTICA* **4**(12), 1526–1533.

Henry, W. (1994), Use of tapered optical fibres as evanescent field sensors, *in* Lieberman, RA, ed., 'Chemical, Biochemical, and Environmental Fiber Sensore VI', Vol. 2293 of *Proceedings of the Society of Photo-Optical Instrumentation Engineers (SPIE)*, SOC Photo OPT Instrumentat Engineers, pp. 2–14. Chemical, Biochemical, and Environmental Fiber Sensors VI Conference, San Diego, CA, JUL 26-27, 1994.

Hodgkinson, J. & Tatam, R. P. (2013), 'Optical gas sensing: a review', *Measurement Science and Technology* **24**(1).

Hosseini, P., Ermolov, A., Tani, F., Novoa, D. & Russell, P. S. J. (2018), 'UV Soliton Dynamics and Raman-Enhanced Supercontinuum Generation in Photonic Crystal Fiber', *ACS Photonics* **5**(6), 2426–2430.

Hoult, T. (2015), Lasers in the 2um SWIR spectral regime and their applications, *in* '2015 Conference on Lasers and Electro-Optics (CLEO). Proceedings', p. 2 pp. 2015 Conference on Lasers and Electro-Optics (CLEO), 10-15 May 2015, San Jose, CA, USA.

Jiang, X., Joly, N. Y., Finger, M. A., Babic, F., Wong, G. K. L., Travers, J. C. & Russell, P. S. J. (2015), 'Deep-ultraviolet to mid-infrared supercontinuum generated in solid-core ZBLAN photonic crystal fibre', *NATURE Photonics* **9**(2), 133–139.

Jin, Q., Yin, T., Tu, Z., Chen, D., Shi, Y., Dai, D. & Gao, S. (2019), 'Performance evaluation of continuous-wave mid-infrared wavelength conversion in silicon waveguides', *Applied Optics* **58**(10), 2584–2588.

Joly, N., Nold, J., Chang, W., Hoelzer, P., Nazarkin, A., Wong, G. K. L., Biancalana, F. & Russell, P. S. J. (2011), 'Bright Spatially Coherent Wavelength-Tunable Deep-UV Laser Source Using an Ar-Filled Photonic Crystal Fiber', *Physical Review Letters* **106**(20).

Kaminski, C. F., Watt, R. S., Elder, A. D., Frank, J. H. & Hult, J. (2008), 'Supercontinuum radiation for applications in chemical sensing and microscopy', *Applied Physics B-Lasers and Optics* **92**(3), 367–378.

Karp, J., Challener, W., Kasten, M., Choudhury, N., Palit, S., Pickrell, G., Homa, D., Floyd, A., Cheng, Y., Yu, F. & Knight, J. (2016), Fugitive methane leak detection using mid-infrared hollow-core photonic crystal fiber containing ultrafast laser drilled side-holes, *in* Udd, E and Pickrell, G and Du, HH, ed., 'Fiber optic sensors and applications XIII', Vol. 9852 of *Proceedings of SPIE*, SPIE, SPIE-INT SOC optical engineering, 1000 20th st, PO BOX 10, Bellingham, WA 98227-0010 USA. Conference on Fiber Optic Sensors and Applications XIII, Baltimore, MD, APR 18-21, 2016.

Knight, J., Birks, T., Russell, P. & Atkin, D. (1997), 'All-silica single-mode optical fiber with photonic crystal cladding: Errata', *Optics Letters* **22**(7), 484–485.

Kracht, D., Sayinc, H., Yilmaz, S., Wysmolek, M., Hausmann, K., Ottenhues, C., Wandt, D., Wienke, A. & Neumann, J. (2016), Innovative laser sources operating around 2 mu m, *in* Schmidt, M and Vollertsen, F and Arnold, CB, ed., 'Laser Assisted Net Shape Engineering 9 International Conference on Photonic Technologies Proceedings of the LANE 2016', Vol. 83 of *Physics Procedia*, Int Acad Prod Engn; Erlangen Grad Sch Adv Opt Technologies; German Acad Soc Prod Engn; German Sci Laser Soc; Bayerisches Laserzentrum Gmbh; Univ Erlangen Nurnberg, Inst Photon Technologies, pp. 1184–1195. 9th International Conference on Photonic Technologies (LANE), Furth, GERMANY, SEP 19-22, 2016.

Kudlinski, A., George, A. K., Knight, J. C., Travers, J. C., Rulkov, A. B., Popov, S. V. & Taylor, J. R. (2006), 'Zero-dispersion wavelength decreasing photonic crystal fibers for ultraviolet-extended supercontinuum generation', *Optics Express* **14**(12), 5715–5722.

Lavoute, L., Knight, J. C., Dupriez, P. & Wadsworth, W. J. (2010), 'High power red and near-IR generation using four wave mixing in all integrated fibre laser systems', *Optics Express* **18**(15), 16193–16205.

Lehmann, H., Bartelt, H., Willsch, R., Amezcua-Correa, R. & Knight, J. C. (2010), Distributed gas sensor based on a photonic bandgap fiber cell with laser-drilled, lateral micro channels, *in* Santos, JL and Culshaw, B and LopezHiguera, JM and MacPherson, WN, ed., 'Fourth European Workshop on Optical Fibre Sensors', Vol. 7653 of *Proceedings of SPIE*, INSEC Porto; Univ Porto; SPIE. Fourth European Workshop on Optical Fibre Sensors, Porto, PORTUGAL, SEP 08-10, 2010.

Leon-Saval, S. G., Birks, T. A., Wadsworth, W. J., Russell, P. S. J. & Mason, M. W. (2004), 'Supercontinuum generation in submicron fibre waveguides', *Optics Express* **12**(13), 2864–2869.

Love, J. D., Henry, W. M., Stewart, W. J., Black, R. J., Lacroix, S. & Gonthier, F. (1991), 'Tapered single-mode fibers and devices .1. Adiabaticity criteria', *Iee Proceedings-J Optoelectronics* **138**(5), 343–354.

Lu, Z. G., Bock, P. J., Liu, J. R., Sun, F. G. & Hall, T. J. (2006), 'All-optical 1550 to 1310 nm wavelength converter', *Electronics Letters* **42**(16), 937–938.

Masum, B. M., Aminossadati, S. M., Leonardi, C. R., Kizil, M. S. & Amanzadeh, M. (2018), 'Numerical analysis of gas diffusion in drilled Hollow-Core Photonic Crystal fibres', *Measurement* **127**, 283–291.

McWilliam, I. & Dewar, R. (1958), 'Flame Ionization Detector for Gas Chromatography', *NATURE* **181**(4611), 760.

Meschede, D. (2017), Light Propagation in Matter: Interfaces, Dispersion, and Birefringence, *in* 'Optics, Light, and lasers: The practical approach to modern aspects of photonics and laser physics', Wiley-V C H Verlag GMBH, Pappelallee 3, W-69469 Weinheim, Germany, pp. 83–120.

Morioka, T., Kawanishi, S., Uchiyama, K., Takara, H. & Sauwatari, M. (1994), 'Polarization-Independent 100 Gbit/s All Optical Demultiplexer Using 4-Wave Mixing in a Polarization Maintaining Fiber Loop', *Electronics Letters* **30**(7), 591–592.

Namihira, Y. (1994), 'Relationship between nonlinear effective area and modefield diameter for dispersion shifted fibers', *Electronics Letters* **30**(3), 262–264.

Nodop, D., Jauregui, C., Schimpf, D., Limpert, J. & Tnnermann, A. (2009), 'Efficient high-power generation of visible and mid-infrared light by degenerate four-wave-mixing in a large-mode-area photonic-crystal fiber', *Optics letters* **34**, 3499–501.

Ortigosa-Blanch, A., Knight, J., Wadsworth, W., Arriaga, J., Mangan, B., Birks, T. & Russell, P. (2000), 'Highly birefringent photonic crystal fibers', *Optics Letters* **25**(18), 1325–1327.

Pliutau, D. & Roslyakov, K. (2017), 'Bytran - spectral calculations for portable devices using the HITRAN database', *Earth Science Informatics* **10**(3), 395–404.

Raj, G. J., Nagarajan, N., Raja, R. V. J. & Ganapathy, R. (2015), Effect of Two Zero Dispersion Wavelengths on Supercontinuum Generation in CS2 Cored Photonic Crystal Fiber, *in* Lakshminarayan, V and Bhattacharya, I, ed., '2015 2nd International Conference on Opto-Electronics and Applied Optics (IEM OPTRONIX)', ieee photonics soc; ieee vancouver sect; ieee; int year of light; optical soc of india. 2nd International Conference on Opto-Electronics and Applied Optics (IEM OPTRONIX 2015), University of British Columbia, Vancouver, Canada, OCT 15-17, 2015.

Ranka, J., Windeler, R. & Stentz, A. (2000), 'Visible continuum generation in air-silica microstructure optical fibers with anomalous dispersion at 800 nm', *Optics Letters* **25**(1), 25–27.

Russell, E., Kavanagh, N., Shortiss, K. & Gunning, F. C. G. (2018), Development of thulium-doped fibre amplifiers for the 2um waveband, *in* Taccheo, S and Mackenzie, JI and Ferrari, M, ed., 'Fiber Lasers and Glass Photonics: Materials Through Applications', Vol. 10683 of *Proceedings of*

SPIE, Strasbourg Eurooptimist; CNRS; Investissements Avenvir; iCube; Univ Strasbourg; SPIE. Conference on Fiber Lasers and Glass Photonics - Materials through Applications, Strasbourg, FRANCE, APR 22-26, 2018.

Sardar, M. R. & Faisal, M. (2017), Gas Sensor Based on Octagonal Hollow Core Photonic Crystal Fiber, *in* '2017 IEEE International Conference on Imaging, Vision & Pattern Recognition (ICIVPR)', IEEE; IEEE Bangladesh Sect; IEEE CS TC Pattern Anal & Machine Intelligence; IEEE SMC TC Med Informat; IEEE SMC TC Visual Analyt & Commun; Int Assoc Pattern Recognit; Inst Ind Applicat Engineers; Univ Dhaka, IEEE Student Branch; DU, IEEE Women Engn Affin Grp; Ctr Nat Sci & Engn Res. IEEE International Conference on Imaging, Vision & Pattern Recognition (icIVPR), Univ Dhaka, Dhaka, Bangladesh, FEB 13-14, 2017.

Shao, M., Qiao, X., Fu, H., Zhao, N., Liu, Q. & Gao, H. (2013), 'An In-Fiber Mach-Zehnder Interferometer Based on Arc-Induced Tapers for High Sensitivity Humidity Sensing', *IEEE Sensors Journal* **13**(5), 2026–2031.

Silfvast, W. (2004), *Laser Fundamentals*, Cambridge University Press.

Skryabin, D. V. & Yulin, A. V. (2005), 'Theory of generation of new frequencies by mixing of solitons and dispersive waves in optical fibers', *Physical Review E* **72**(1).

Stoicheff, B. (1963), 'Characteristics of Stimulated Raman Radiation Generated by Coherent Light', *Physics Letters* **7**(3), 186–188.

Stone, J., Wadsworth, W. & Gerke, T. (2016), 'Photonic crystal fibers advance supercontinuum generation', *Laser Focus World* **52**(6), 45+.

Swiderski, J., Michalska, M. & Grzes, P. (2018), 'Broadband and top-flat mid-infrared supercontinuum generation with 3.52 W time-averaged power in a ZBLAN fiber directly pumped by a 2-A mu m mode-locked fiber laser and amplifier', *Applied Physics B-Lasers and Optics* **124**(7).

Sysoliatin, A. A., Senatorov, A. K., Konyukhov, A. I., Melnikov, L. A. & Stasyuk, V. A. (2007), 'Soliton fission management by dispersion oscillating fiber', *Optics Express* **15**(25), 16302–16307.

Takara, H., Ohara, T., Yamamoto, T., Masuda, H., Abe, M., Takahashi, H. & Morioka, T. (2005), 'Field demonstration of over 1000-channel DWDM transmission with supercontinuum multi-carrier source', *Electronics Letters* **41**(5), 270–271.

Teipel, J., Turke, D., Giessen, H., Zintl, A. & Braun, B. (2005), 'Compact multi-Watt picosecond coherent white light sources using multiple-taper fibers', *Optics Express* **13**(5), 1734–1742.

Testa, G., Persichetti, G. & Bernini, R. (2018), 'Hollow-Core-Integrated Optical Waveguides for Mid-IR Sensors', *IEEE Journal of Selected Topics in Quantum Electronics* **24**(6).

the PNNL database (2009), 'Ftir infrared cross-sections for methane. taken from the pacific northwest national lab (pnnl).'.
URL: *http://vpl.astro.washington.edu/spectra/ch4.htm*

Thiel, C. (2000), 'Four-wave mixing and its applications'.

Thurbide, K. & Hayward, T. (2004), 'Improved micro-flame detection method for gas chromatography', *Analytica Chimica Acta* **519**(1), 121–128.

Tipler, P. & Mosca, G. (2007), *Physics for Scientists and Engineers*, Physics for Scientists and Engineers: Standard, W. H. Freeman.

Tong, L. M., Lou, J. Y. & Mazur, E. (2004), 'Single-mode guiding properties of subwavelength-diameter silica and silicon wire waveguides', *Optics Express* **12**(6), 1025–1035.

Urich, A., Maier, R. R. J., Mangan, B. J., Renshaw, S., Knight, J. C., Hand, D. P. & Shephard, J. D. (2012), 'Delivery of high energy Er:YAG pulsed laser light at 2.94 mu m through a silica hollow core photonic crystal fibre', *Optics Express* **20**(6), 6677–6684.

Wadsworth, W., Joly, N., Knight, J., Birks, T., Biancalana, F. & Russell, P. (2004), 'Supercontinuum and four-wave mixing with Q-switched pulses in endlessly single-mode photonic crystal fibres', *Optics Express* **12**(2), 299–309.

Wai, P. K. A., Menyuk, C. R., Lee, Y. C. & Chen, H. H. (1986), ' Nonlinear pulse-propagation in the neighborhood of the zero-dispersion wavelength of monomode optical fibers', *Optics Letters* **11**(7), 464–466.

Wang, P., Murugan, G. S., Brambilla, G., Ding, M., Semenova, Y., Wu, Q. & Farrell, G. (2012), 'Chalcogenide Microsphere Fabricated From Fiber Tapers Using Contact With a High-Temperature Ceramic Surface', *IEEE Photonics Technology Letters* **24**(13), 1103–1105.

Wang, S., Huang, H., Liu, X., Chen, H., Zhou, W., Liu, S. & Shen, D. (2019), 'Rhenium diselenide as the broadband saturable absorber for the nanosecond passively Q-switched thulium solid-state lasers', *Optical Materials* **88**, 630–634.

Wang, Y., Dai, S., Peng, X., Zhang, P., Wang, X. & You, C. (2018), 'Mid-infrared supercontinuum generation spanning from 1.9 to 5.7 mu m in a chalcogenide fiber taper with ultra-high NA', *Infrared Physics & Technology* **88**, 102–105.

Wilson, Witkowska, A., Lai, K., Leon-Saval, S. G., Wadsworth, W. J. & Birks, T. A. (1975), 'Tapered optical directional coupler', *IEEE Transactions on Microwave Theory and Techniques* **MT23**(1), 85–92.

Witkowska, A., Lai, K., Leon-Saval, S. G., Wadsworth, W. J. & Birks, T. A. (2006), 'All-fiber anamorphic core-shape transitions', *Optics Letters* **31**(18), 2672–2674.

Wojcik, J., Urbanczyk, W., Bock, W., Janoszczyk, B., Mergo, P., Makara, M., Poturaj, K. & Spytek, W. (1999), Prototype of the side-hole HB optical fiber, *in* Dorosz, J and Romaniuk, RS, ed., 'Optical Fibers and their Applications VI', Vol. 3731 of *Proceedings of the Society of Photo-Optical Instrumentation Engineers (SPIE)*, Mil Univ Technol, Inst Optoelectr, Poland; Biaglass Co, Poland; Polish Acad Sci, Comm Electr & Telecommun, Sect Optoelectr; Assoc Polish Elect Engineers, Polish Comm Optoelectr; SPIE Poland Chapter; Tech Univ Nialystok, Poland, pp. 88–93. Conference on the Optical Fibers and Their Applications VI, Bialowleza, Poland, JAN 22-24, 1998.

Wu, Y., Yao, B., Zhang, A., Rao, Y., Wang, Z., Cheng, Y., Gong, Y., Zhang, W., Chen, Y. & Chiang, K. S. (2014), 'Graphene-coated microfiber Bragg grating for high-sensitivity gas sensing', *Optics Letters* **39**(5), 1235–1237.

Yang, F., Jin, W., Cao, Y. & Ho, H. L. (2014), Hollow-core photonic bandgap fiber gas sensor with high sensitivity and fast response, *in* LopezHiguera, JM and Jones, J and LopezAmo, M and Santos, JL, ed., '23RD International Conference on Optical Fibre Sensors', Vol. 9157 of *Proceedings of SPIE*, Univ Cantabria, Grupo Ingn Fotonica; SPIE; Opt Soc; IEEE Photon Soc; Japan Soc Appl Phys; EIC; SICE; Gobierno Espana; Gobierno Cantabria, Consejeria Innovac Industria, Turismo & Comercio; Cantabria Infinita; Univ Cantabria, Cantabria Campus Internac; Ayuntamiento Santander; Ayuntamiento Ramales Victoria; COPSESA; OZ Opt Ltd; Bay Spec; Fibersensing; Fibercore Ltd; Bandweaver Technologies Co Ltd; NBG Syst GmbH; Fiberguide Ind Inc; NKT Photon; Innovat Econ; Innovat Photon Technol; Luna; Focus. 23rd International Conference on Optical Fibre Sensors, Santander, SPAIN, JUN 02-06, 2014.

Yang, F., Jin, W., Lin, Y., Wang, C., Lut, H. & Tan, Y. (2017), 'Hollow-Core Microstructured Optical Fiber Gas Sensors', *Journal of Lightwave Technology* **35**(16), 3413–3424.

Yarrow, M. J., Wadsworth, W. J., Lavoute, L., Clowes, J. R. & Grudinin, A. B. (2012), Power-scalable tunable UV, visible, and NIR generation from an ultrafast fiber OPA based on four wave mixing in PCF, *in* Vodopyanov, KL, ed., 'Nonlinear Frequency Generation and Conversion: Materials, Devices, and Applications XI', Vol. 8240 of *Proceedings of SPIE*, SPIE. Conference on

Nonlinear Frequency Generation and Conversion - Materials, Devices, and Applications XI, San Francisco, CA, JAN 24-26, 2012.

Ye, J., Schnatz, H. & Hollberg, L. (2003), 'Optical frequency combs: From frequency metrology to optical phase control', *IEEE Journal of Selected Topics in Quantum Electronics* **9**(4), 1041–1058.

Yokota, H., Sugai, E. & Sasaki, Y. (1997), 'Optical irradiation method for fiber coupler fabrications', *Optical Review* **4**(1A), 104–107.

Yu, F., Wadsworth, W. J. & Knight, J. C. (2012), 'Low loss silica hollow core fibers for 3-4 mu m spectral region', *Optics Express* **20**(10), 11153–11158.

Yu, X. J., Diao, C. Z., Venkatesan, T., Breese, M. B. H. & Rusydi, A. (2018), 'A soft x-ray-ultraviolet (SUV) beamline and diffractometer for resonant elastic scattering and ultraviolet-vacuum ultraviolet reflectance at the Singapore synchrotron light source', *Review of Scientific Instruments* **89**(11).

Zhang, L., Tuan, T. H., Kawamura, H., Nagasaka, K., Suzuki, T. & Ohishi, Y. (2016), Femtosecond Four-Wave Mixing from Near-Infrared to Mid-Infrared in a Tellurite Step-Index Fiber, *in* '2016 Conference on Lasers and Electro-Optics (CLEO)', Conference on Lasers and Electro-Optics. Conference on Lasers and Electro-Optics (CLEO), San Jose, CA, JUN 05-10, 2016.

Zimmermann, S., Wischhusen, S. & Muller, J. (2000), 'Micro flame ionization detector and micro flame spectrometer', *Sensors and Actuators B-Chemical* **63**(3), 159–166.

Zuo, P., Fuji, T. & Suzuki, T. (2010), 'Spectral phase transfer to ultrashort UV pulses through four-wave mixing', *Optics Express* **18**(15), 16183–16192.